

What next for the CMSSM and the NUHM: improved prospects for superpartner and dark matter detection

Leszek Roszkowski,¹ Enrico Maria Sessolo and Andrew J. Williams

*National Centre for Nuclear Research,
Hoża 69, 00-681 Warsaw, Poland*

E-mail: L.Roszkowski@sheffield.ac.uk,
Enrico-Maria.Sessolo@fuw.edu.pl, Andrew.Williams@fuw.edu.pl

ABSTRACT: We present an updated analysis of the CMSSM and the NUHM using the latest experimental data and numerical tools. We map out favored regions of Bayesian posterior probability in light of data from the LHC, flavor observables, the relic density and dark matter searches. We present some updated features with respect to our previous analyses: we include the effects of corrections to the light Higgs mass beyond the 2-loop order using `FeynHiggs 2.10.0`; we include in the likelihood the latest limits from direct searches for squarks and gluinos at ATLAS with $\sim 20 \text{ fb}^{-1}$; the latest constraints on the spin-independent scattering cross section of the neutralino from LUX are applied taking into account uncertainties in the nuclear form factors. We find that in the CMSSM the posterior distribution now tends to favor smaller values of M_{SUSY} than in the previous analyses. As a consequence, the statistical weight of the A -resonance region increases to about 30% of the total probability, with interesting new prospects for the 14 TeV run at the LHC. The most favored region, on the other hand, still features multi-TeV squarks and gluinos, and $\sim 1 \text{ TeV}$ higgsino dark matter whose detection prospects by current and one-tonne detectors look very promising. The same region is predominant in the NUHM, although the A -resonance region is also present there as well as a new solution, of neutralino-stau coannihilation through the channel $\tilde{\tau}\tilde{\tau} \rightarrow hh$ at very large μ . We derive the expected sensitivity of the future CTA experiment to $\sim 1 \text{ TeV}$ higgsino dark matter for both models and show that the prospects for probing both models are realistically good. We comment on the complementarity of this search to planned direct detection one-tonne experiments.

¹On leave of absence from the University of Sheffield, U.K.

Contents

1	Introduction	1
2	Scanning methodology and experimental constraints	3
3	Results in the CMSSM	9
3.1	Posterior distributions and prospects for collider searches	9
3.2	Prospects for dark matter detection	15
4	Results in the NUHM	17
4.1	Posterior distributions and prospects for collider searches	17
4.2	Prospects for dark matter detection	23
5	Summary and conclusions	24
A	Impact of a recent calculation of the sensitivity of CTA	26

1 Introduction

The recent discovery of a Higgs boson at the LHC [1, 2] raised widespread excitement in the particle physics community and spurred a lot of activity to interpret the new discovery in the context of the Standard Model (SM) and models of new physics. In particular, the mass of the newly discovered particle, $m_h \simeq 126$ GeV, is well within (albeit on the upper side) the predictions of low-scale supersymmetry (SUSY). In fact, since in SUSY the quartic coupling of the scalar potential is related to the gauge couplings of the electroweak (EW) sector, the lightest Higgs mass can deviate from the masses of the W and Z bosons only through radiative corrections so that its value is effectively bounded to be less than about 135 GeV.

The implications of the Higgs discovery for the parameter space of the popular Constrained Minimal Supersymmetric Standard Model (CMSSM) [3] and Non-Universal Higgs Model (NUHM), have been intensely investigated (see, e.g., [4–18] for some of the papers that followed the Higgs discovery). Many of those studies, including our own ones, explored statistical combinations of the constraints from the Higgs measurements at the LHC with other pieces of experimental information: the measurement of the dark matter relic density [19]; a number of EW precision observables; measurements of rare-decay branching ratios like $\text{BR}(\bar{B} \rightarrow X_s \gamma)$ [20], $\text{BR}(B_u \rightarrow \tau \nu)$ [21], or the recent measurement of a SM-like $\text{BR}(B_s \rightarrow \mu^+ \mu^-)$ at the LHC [22, 23]; the anomalous magnetic moment of the muon [24, 25], etc. Additional constraints came from direct SUSY searches at the LHC. For instance, in our previous CMSSM and NUHM analyses [11, 16] the likelihood function included limits from the CMS razor 4.4 fb^{-1} analysis at 7 TeV [26] and the CMS α_T 11.7 fb^{-1}

analysis at 8 TeV [27], which were obtained by simulating the SUSY signal and detector response and comparing them to the observed and background yields in different channels given by the experimental collaboration.

It is important to point out that, besides the Higgs boson mass measurement and LHC direct bounds, the constraint showing by far the strongest impact on the parameter space of the Minimal Supersymmetric SM (MSSM) is the relic density. It is measured very precisely and its value tends to be too large in broad regions of the parameter space. The mechanisms for reducing the relic abundance are quite general and insensitive to the particular pattern of scalar mass unification with the exception, obviously, of solutions requiring the presence of light sleptons, which in the CMSSM/NUHM are excluded by direct LHC limits on the squarks. In other words, while featuring a limited number of free parameters that make them more predictive than general phenomenological parametrizations defined at the scale of the lightest SUSY partners, the CMSSM and the NUHM produce solutions to the relic density that are present and play an important role in more general models. From this point of view, the CMSSM ansatz and its most immediate extension, the NUHM, are very useful frameworks to investigate the predictions for dark matter in constrained frameworks within the MSSM with gaugino unification at the GUT scale.

The picture that emerged particularly in the analyses [15, 16] for the CMSSM and [14, 16] for the NUHM, is that the relatively large value of the Higgs mass, the SM-like nature of its couplings to the other SM particles, the measured values of the flavor physics observables in great agreement with the SM, and the non-observation of SUSY particles below $\sim 1 - 1.5$ TeV at the LHC, can all be easily accommodated in an extended region of the parameter space characterized by squarks and gluinos in the multi-TeV regime and the heavy Higgs sector effectively decoupled. In this region, the relic density can naturally assume the value measured by PLANCK, as the lightest SUSY particle (LSP) is an almost pure higgsino neutralino with a mass $m_\chi \simeq 1$ TeV.¹ The existence of the ~ 1 TeV higgsino solution for DM in the MSSM has been long known [28, 29] but in the framework of unified SUSY was first pointed out in a pre-LHC study of the NUHM [30].

Interestingly, parameter space regions with sparticles in the multi-TeV regime and ~ 1 TeV higgsino dark matter in agreement with the value of the relic density were shown to be very favored also in scans of the phenomenological MSSM [31], in the Next-to-Minimal Supersymmetric SM [32], and in a variety of models with non-universal boundary conditions at the GUT scale [33]. Incidentally, it was shown in [33] that for some of these models focus point-like mechanisms significantly increase the naturalness of the ~ 1 TeV higgsino region with respect to the CMSSM, without affecting dark matter properties and prospects for detection. As a matter of fact, the best prospects for detection of the ~ 1 TeV higgsino region indeed come from dark matter direct detection experiments, particularly at 1-tonne detectors, as the spin-independent neutralino-proton cross section, σ_p^{SI} , is well

¹While other regions of the parameter space, characterized by bino dark matter and such that the relic abundance is saturated through mechanisms of A -resonance or stau co-annihilation, are consistent with the constraints at the 1 or 2σ level, the ~ 1 TeV higgsino region shows by far the best agreement with all of them with the exception of $\delta(g-2)_\mu$, which favors low M_{SUSY} below ATLAS/CMS bounds in unified models.

within the projected sensitivities of the currently running and future 1-tonne experiments.

Also very interestingly, recent studies of the sensitivity of the Cherenkov Telescope Array (CTA) [34] show the largest projected reach in the region characterized by dark matter mass and annihilation cross section typical of the ~ 1 TeV higgsino region [35, 36], thus opening up the enticing possibility of complementary detection for these scenarios.

On the other hand, the statistical analyses of Refs. [9–16] were based on the calculation of the Higgs mass performed at two loops, implemented in the most popular SUSY spectrum calculators [37–39] or in earlier versions of `FeynHiggs` [40–43]. Significant effort in the direction of improving the theoretical precision of the Higgs mass calculation in the MSSM [44–48] has recently prompted some groups to update their previous analyses [49–51]. Reference [51] in particular shows the first global statistical analysis to incorporate these recent developments in a frequentist approach.

In this paper, we update the global Bayesian analyses of the CMSSM and the NUHM previously produced by our group, by including the following new elements:

- We calculate the Higgs mass with `FeynHiggs` 2.10.0 [47], which incorporates results beyond two loops with a resummation of leading and sub-leading logarithms in the top/stop sector.
- We update the likelihood map for direct SUSY searches with the most constraining limits from ATLAS with 20 fb^{-1} at 8 TeV.
- We include the recent constraints from the LUX experiment [52] in the likelihood function.
- We add an analysis of the prospect for CTA to independently explore the favored regions.

We will focus in particular on the properties of the regions that present the highest posterior probability, favored by the value of the dark matter relic density. We will show that the bulk of the posterior still lies on the ~ 1 TeV higgsino region, but in the CMSSM its statistical significance is not as overwhelmingly predominant as previously shown. We will touch on the prospects for detection at the LHC and in future colliders, but will focus particularly on dark matter searches like the above-mentioned 1-tonne detectors and the CTA.

The paper is organized as follows. In Sec. 2 we describe the statistical setup, the constraints included in the likelihood function, the parameter prior ranges and distributions, and the numerical tools used in our scans. In Sec. 3 we present the results of the Bayesian analysis of the CMSSM, including prospects at collider and dark matter experiments. In Sec. 4 we present equivalent results for the NUHM. We give our summary and conclusions in Sec. 5.

2 Scanning methodology and experimental constraints

Our goal is to determine the regions in the parameter space of the CMSSM and the NUHM that are favored by all of the experimental data available. We follow a Bayesian approach outlined in [11, 16, 53, 54] and map out the 68% and 95% credible regions in

two-dimensional (2D) projections of the marginalized posterior probability density function (pdf) and/or the one-dimensional (1D) marginalized pdf of some interesting parameters. The posterior pdf (or, simply, the posterior), $p(m|d)$, is given by Bayes' Theorem,

$$p(m|d) = \frac{p(d|m)\pi(m)}{p(d)}, \quad (2.1)$$

where m is the set of model parameters, $\pi(m)$ is prior probability distribution of the parameters m , $p(d|m) \equiv \mathcal{L}(m)$ is the probability of obtaining the experimental data d given the model parameters, known as the likelihood function, and $p(d)$ is a normalization factor called the evidence, which is required for the comparison of different models. In this framework the likelihood function encodes all of our information from experimental constraints and their associated uncertainties.

We can consider marginalized posterior distributions of subsets of the parameters m by integrating over the remaining parameters. The posterior distribution of a subset of parameters $\psi_{1\dots r}$ from the full set of parameters $m_{1\dots N}$ is then given by

$$p(\psi_{1\dots r}|d) = \int p(m|d) d^{N-r} m. \quad (2.2)$$

This leads to a natural prescription for dealing with nuisance parameters, since these can be included as parameters of the model with suitable prior probability distributions and then marginalized over to obtain posterior distributions of the parameters of interest.

We construct the likelihood function from the experimental data. We account for positive measurements with a gaussian likelihood function and combine experimental and theoretical errors in quadrature. A summary of the experimental constraints used in this analysis is given in Table 1. In addition, we adopt a specific procedure for incorporating the constraints from Higgs boson searches at the LHC, direct searches for SUSY, and the constraints from dark matter direct detection at LUX.

The discovery of a SM-like Higgs boson with $m_h \simeq 126$ GeV presents a challenging constraint. The experimental collaborations have published the Higgs signal rates in several channels and we make use of this information by interfacing with the public code **HiggsSignals** v1.0.0 [55]. We supply **HiggsSignals** with the Higgs boson production cross section and branching ratios calculated by **FeynHiggs** [40–43] and use the calculated χ^2 result in the likelihood function. An accurate prediction for the lightest Higgs boson is important due to the small width of the observed experimental signal. Recently [47] **FeynHiggs** v2.10.0 has incorporated results beyond two loops with a resummation of leading and sub-leading logarithms in the top/stop sector. We include these in our scan. We fix the uncertainty in the mass of the lightest Higgs to 2 GeV, as a conservative estimate of the remaining sources of theory error. As well as the observed signal at ~ 126 GeV, Higgs searches in other mass ranges may constrain the heavy Higgs bosons. We use **HiggsBounds** v4.1.0 [56–58] to reject points excluded at 95% C.L. by those searches.

The contribution to the likelihood arising from the results of the LUX experiment [52] is derived as was explained in [33], i.e., by applying the procedure developed in Ref. [69]

Constraint	Mean	Exp. Error	Th. Error	Ref.
Higgs sector	See text.	See text.	See text.	[55–58]
Direct SUSY searches	See text.	See text.	See text.	[59–67]
σ_p^{SI}	See text.	See text.	See text.	[52]
$\Omega_\chi h^2$	0.1199	0.0027	10%	[19]
$\sin^2 \theta_{\text{eff}}$	0.23155	0.00015	0.00015	[68]
$\delta(g-2)_\mu \times 10^{10}$	28.7	8.0	1.0	[24, 25]
$\text{BR}(\bar{B} \rightarrow X_s \gamma) \times 10^4$	3.43	0.22	0.21	[20]
$\text{BR}(B_u \rightarrow \tau \nu) \times 10^4$	0.72	0.27	0.38	[21]
ΔM_{B_s}	17.719 ps ⁻¹	0.043 ps ⁻¹	2.400 ps ⁻¹	[68]
M_W	80.385 GeV	0.015 GeV	0.015 GeV	[68]
$\text{BR}(B_s \rightarrow \mu^+ \mu^-) \times 10^9$	2.9	0.7	10%	[22, 23]

Table 1: The experimental constraints used in this study.

for the likelihood of XENON100 [70] to the data from LUX. We assume that the number of observed events follows a Poisson distribution centered on the predicted signal plus background. A likelihood map in the $(m_\chi, \sigma_p^{\text{SI}})$ plane is generated by simulating signal events in **micrOMEGAs** [71] and marginalizing over the uncertainty in the expected number of background events. In Fig. 1(a) we plot the 68.3%, 90%, and 99.7% C.L. exclusion bounds obtained with our procedure. The dashed black line gives the official 90% C.L. exclusion bound. In our scans, we also account for uncertainties in the predicted elastic scattering cross section [72, 73] by including the nuclear form factors σ_s and $\Sigma_{\pi N}$ as nuisance parameters.

We finally account for the direct SUSY searches at the LHC by updating the method developed in [11, 16]. We generate a grid in the $(m_0, m_{1/2})$ plane at 50-GeV intervals. At each point we generate squark- and gluino-production events using **Madgraph** [74] and produce the parton shower in **pythia** [75]. The cross sections are calculated using **nll-fast** [76–80] to include the next-to-leading order and next-to-leading log contributions. We evaluate the expected number of events in a given signal region for the searches considered using **CheckMATE** [59–67]. **CheckMATE** includes a number of validated SUSY searches and includes an advanced tuning of the fast detector simulation. We calculate a likelihood for each search from the product of Poisson distributions for each signal region. We account for the uncertainties in the background rate by marginalizing over the background rate with a gaussian distribution. When calculating the likelihood, we consider the two searches that give the strongest limits in the CMSSM: a 0 lepton 2–6 jets ATLAS search [81] and a 0–1 lepton 3 b -jets ATLAS search [82]. We scale the total squark and gluino production rate by a small constant factor to match the limit achieved by the experimental analyses in order to account for the remaining differences in efficiencies due to the fast detector simulation. To combine the results of the two ATLAS searches we evaluate at each point which of the two searches has the largest expected exclusion and then use that search to

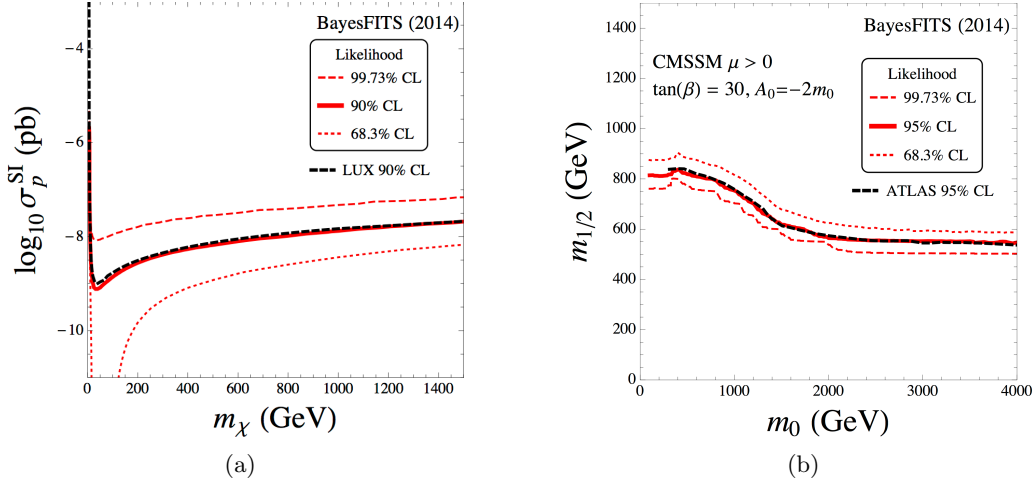


Figure 1: (a) The 68.3% C.L. (red dotted line), 90% C.L. (red solid line) and 99.7% C.L. (red dashed line) exclusion bounds given by our likelihood map for dark matter direct detection experiments, compared with the 90% C.L. limit published by LUX [52] (black dashed line). (b) The 68.3% C.L. (red dotted line), 95% C.L. (red solid line) and 99.7% C.L. (red dashed line) exclusion bounds for our combination of the ATLAS searches compared to the original 95% C.L. contour from ATLAS (black dashed line).

calculate the likelihood for that point. The combination of the two searches compared to the official 95% C.L. line from ATLAS (where we have combined the lines from the two different searches) is shown in Fig. 1(b). The agreement is very good across the entire range of m_0 and $m_{1/2}$.

In this study, we also estimate the sensitivity of the Cherenkov Telescope Array (CTA) [34] for the favored parameter space of the CMSSM and the NUHM. The results will be shown in Sec. 3.2 and Sec. 4.2, respectively.

The CTA project will build the next generation air Cherenkov telescope observatory. For dark matter masses greater than ~ 100 GeV CTA is expected to significantly exceed current experimental limits for dark matter annihilations such as those from HESS [83] and Fermi-LAT [84]. CTA may even probe cross sections below the canonical thermal relic value for some final states [36].

Reference [36] estimated the future sensitivity of CTA to dark-matter annihilation in the Galactic Center (GC) for the final states $b\bar{b}$, $\mu^+\mu^-$ and $\tau^+\tau^-$ assuming 500 hours of observation time. In order to directly apply their limits to more generic neutralino annihilations, whose final states also include gauge bosons, ZZ and W^+W^- , we infer from [36] the 95% C.L. limit on the expected flux of signal photons per J -factor, $N_{\gamma,95}$, by convolving the photon flux with the effective area given in [85] in a single energy bin between 30 GeV and the dark matter mass:

$$N_{\gamma,95} = t_{\text{obs}} \frac{\langle \sigma v \rangle_{95}^{(b\bar{b}, \mu^+\mu^-, \tau^+\tau^-)}}{8\pi m_\chi^2} N_{\gamma,\text{obs}} J_{\text{fact}}, \quad (2.3)$$

where t_{obs} is the observation time, $\langle \sigma v \rangle_{95}$ is the projected 95% C.L. limit for each final

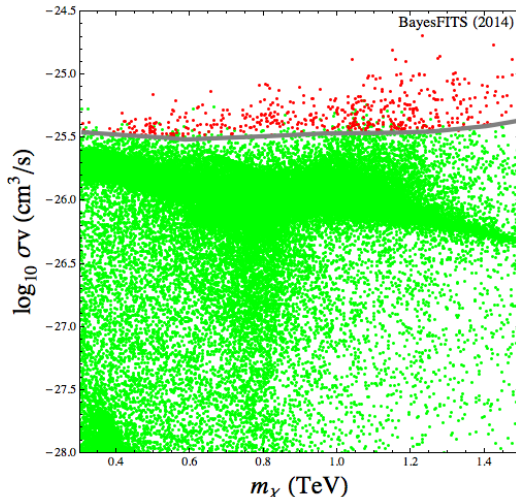


Figure 2: Our indicative 95% C.L. projected sensitivity in the $(m_\chi, \sigma v)$ plane of the MSSM for 500 h of observation at CTA is shown as a gray solid line. The red (dark) points are excluded at the 95% C.L. through direct comparison with $N_{\gamma,95}$, which we derived from the projected bounds given in [36] for different annihilation final states. The gray line marks the maximum cross section bound, which for each point depends on the individual final states.

state, and $N_{\gamma,\text{obs}}$ is given by

$$N_{\gamma,\text{obs}} = \int_{30 \text{ GeV}}^{m_\chi} \frac{dN_\gamma(E)}{dE} A_{\text{eff}}(E) dE, \quad (2.4)$$

where A_{eff} is the effective area, $dN_\gamma(E)/dE$ is the energy spectrum per annihilation and for simplicity we have neglected the effect of finite energy resolution. For validation, one must make sure that the $N_{\gamma,95}$ obtained from the different final-state bounds of [36] are all in very good agreement.

Once $N_{\gamma,95}$ is derived, the photon flux is calculated point by point in our scans using `micrOMEGAs`. In Fig. 2 we show the approximate 95% C.L. limit in the plane of the annihilation cross section times velocity at zero momentum, $\sigma v \equiv \lim_{p \rightarrow 0} \langle \sigma v \rangle$, versus the neutralino mass, m_χ . The limit is extracted by testing each point against the expected $N_{\gamma,95}$, and showing them in red if they are excluded. The large statistical sample shown in Fig. 2 includes the scans performed for this study and those used in [31].

Note that the limit is derived for the photon flux, so that there is no corresponding clear-cut limit in σv . Nevertheless, we show with a gray solid line the maximum extent that can be probed with this method, and we will apply the obtained limit to the figures in Sec. 3.2 and Sec. 4.2.

The scans in this study are performed with the BayesFITS package [11, 16, 31, 86], which interfaces several publicly available tools to direct the scanning procedure and calculate physical observables. The sampling is performed by MultiNest [87] with 4000 and 10000 live points for the CMSSM and NUHM respectively. The evidence tolerance is set to 0.5 and the sampling efficiency to 0.8 for all the scans. We use `SoftSusy v.3.3.9` [37]

Parameter	Description	Range	Distribution
m_0	Universal scalar mass	0.1, 20	Log
$m_{1/2}$	Universal gaugino mass	0.1, 10	Log
A_0	Universal trilinear coupling	-20, 20	Linear
$\tan \beta$	Ratio of the Higgs vevs	3, 62	Linear
$\text{sgn } \mu$	Sign of the Higgs/higgsino mass parameter	+1 or -1	
$m_{H_d}^2 / \sqrt{ m_{H_d}^2 }^{(*)}$	Signed GUT-scale soft mass of H_d	-20, 20	Linear
$m_{H_u}^2 / \sqrt{ m_{H_u}^2 }^{(*)}$	Signed GUT-scale soft mass of H_u	-10, 10	Linear
Nuisance parameter	Description	Central value	Distribution
M_t	Top quark pole mass	$173.34 \pm 0.76 \text{ GeV}$ [90]	Gaussian
$m_b(m_b)^{MS}$	Bottom quark mass	$4.18 \pm 0.03 \text{ GeV}$ [68]	Gaussian
$\alpha_s(M_Z)^{MS}$	Strong coupling	0.1185 ± 0.0006 [68]	Gaussian
$1/\alpha_{\text{em}}(M_Z)^{MS}$	Reciprocal of electromagnetic coupling	127.944 ± 0.014 [68]	Gaussian
$\Sigma_{\pi N}$	Nucleon sigma term	$34 \pm 2 \text{ MeV}$ [71]	Gaussian
σ_s	Strange sigma commutator	$42 \pm 5 \text{ MeV}$ [71]	Gaussian

(*) These quantities are independently scanned in the NUHM analysis.

Table 2: Prior distributions of the CMSSM and nuisance parameters used in the scans. All dimensionful parameters are given in TeV unless indicated otherwise.

to calculate the mass spectrum. As was explained above, this is passed via the SUSY LesHouches Accord format to **FeynHiggs** v.2.10.0 to calculate the higher-order corrections to the Higgs mass. **FeynHiggs** is interfaced with **HiggsSignals** and **HiggsBounds** to evaluate the constraints on the Higgs sector. **SuperISO** v.3.3 [88] is used to calculate $\text{BR}(\bar{B} \rightarrow X_s \gamma)$, $\text{BR}(B_s \rightarrow \mu^+ \mu^-)$,² $\text{BR}(B_u \rightarrow \tau \nu)$, and $\delta(g-2)_\mu$. The observables M_W , $\sin^2 \theta_{\text{eff}}$, ΔM_{B_s} are calculated using **FeynHiggs**. The dark matter observables $\Omega_\chi h^2$, σ_p^{SI} , and σv are computed using **micrOMEGAs** v.3.5.5 [71].

The prior distributions of the model and nuisance parameters for the CMSSM are given in Table 2. Additionally the parameters scanned in the NUHM are indicated with an asterisk. The sign of μ is fixed for each scan. Note that for $\tan \beta < 3$ it becomes very difficult to obtain at the same time EWSB, the correct value of the relic density, or the correct Higgs mass, as the parameters m_{H_u} , m_{H_d} , $\tan \beta$, and the one-loop tadpole corrections must be fine-tuned very precisely. Note also that for the scans with $\mu < 0$ we do not include $\delta(g-2)_\mu$ in the likelihood as it is known to be poorly fitted. We use logarithmic priors for the universal mass parameters m_0 and $m_{1/2}$ to reduce volume effects.

²We use the *non* time-averaged output of **SuperISO**, as explained in [31]. It is numerically closer to the time-averaged SM prediction of Ref. [89] than the code's own time-averaged calculation.

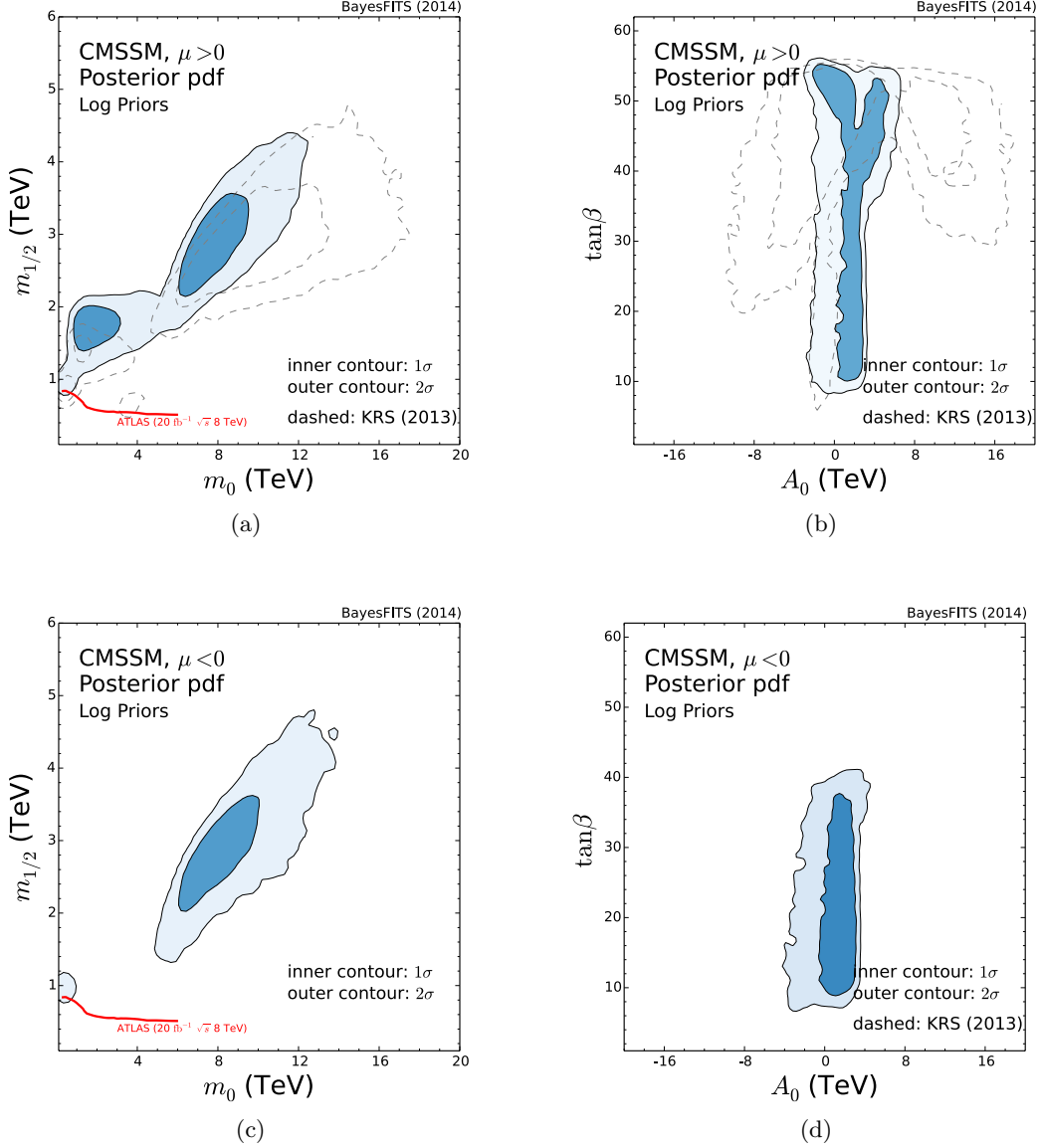


Figure 3: Marginalized 2D posterior distribution for the CMSSM in (a) the $(m_0, m_{1/2})$ plane for $\mu > 0$, (b) the $(A_0, \tan\beta)$ plane for $\mu > 0$, (c) the $(m_0, m_{1/2})$ plane for $\mu < 0$, and (d) the $(A_0, \tan\beta)$ plane for $\mu < 0$. The 68% credible regions are shown in dark blue and the 95% credible regions in light blue. For comparison we show the 68% and 95% credible regions of [16] (KRS (2013) hereafter) encapsulated by thin gray dashed lines. The ATLAS 95% C.L. exclusion line is shown as a red solid line for reference.

3 Results in the CMSSM

3.1 Posterior distributions and prospects for collider searches

In Fig. 3(a) we show the 68% and 95% credible regions of the marginalized 2D pdf in the $(m_0, m_{1/2})$ plane of the CMSSM, for $\mu > 0$. The gray dashed contours mark the previous 68% and 95% regions obtained in [16], which we present for comparison to highlight the

impact of the new more precise calculation of m_h and the new improved constraints.

As has been long standing practice, in the CMSSM the modes of the posterior pdf are identified according to the respective mechanisms to satisfy the relic density constraint. The little, round, 95% credibility region just above the ATLAS line at low m_0 is the stau-coannihilation region [91]; the large region immediately above it, for $m_0 \lesssim 5$ TeV and $m_{1/2} \gtrsim 1.2$ TeV is the A -resonance region [92]; the remaining mode for $m_0 > 5$ TeV and $m_{1/2} \gtrsim 1.5$ TeV is the above-mentioned ~ 1 TeV higgsino region.

The different shape of the present pdf relative to the one given in [16] is due to the new higher-order determination of the Higgs mass. Over the whole parameter space, given equivalent $M_{\text{SUSY}} = (m_{\tilde{t}_1} m_{\tilde{t}_2})^{1/2}$, the value of the Higgs mass has increased by about 2 GeV. In practice, this means that in the ~ 1 TeV higgsino region, where the Higgs mass constraint is always more easily satisfied thanks to the large scalar masses, the favored m_0 values are now limited to less than 12 TeV, above which the Higgs mass becomes too heavy. In the A -resonance and stau-coannihilation regions, the Higgs mass value has increased from an average 122–123 GeV to values closer to 126 GeV, thus improving the χ^2 . As a consequence, the statistical weight of the A -resonance region has now much increased, with new, improved prospects for collider phenomenology, as we shall see later.

In spite of higher mass values for the Higgs boson, the stau-coannihilation region is now becoming disfavored by increasing tension with direct SUSY limits at the LHC, and it will be most likely probed in its entirety in the 14 TeV run. Note also that, with respect to [16], the focus point region [93–95], which is shown in Fig. 3(a) as a 95% dashed contour just above the ATLAS line at $m_0 \simeq 4$ TeV, is now disfavored. Interestingly enough, the new estimate for the Higgs mass in the focus point region is now much closer to the experimental value than before, but the region is disfavored by the LUX results: as is well known, the neutralino there is a mixed composition of bino and higgsino with a mass of $m_\chi \lesssim 600$ GeV. Its large σ_p^{SI} is now excluded by LUX at 90% C.L. We will come back to this point in Sec. 3.2.

In Fig. 3(b) we show the credible regions of the 2D pdf in the $(A_0, \tan \beta)$ plane of the CMSSM, for $\mu > 0$. The three favored modes of the posterior are not as clearly separated as in Fig. 3(a), or as they were in the $(A_0, \tan \beta)$ plane shown in [16]. One can now recognize an elongated 68% credible region for $0 \lesssim A_0 \lesssim 2$ TeV and $8 \lesssim \tan \beta \lesssim 45$, which belongs to the ~ 1 TeV higgsino region and extends to slightly larger, positive A_0 values for $\tan \beta \gtrsim 45$. An elongated 95% credible area is adjacent to it to the left: it encompasses part of the ~ 1 TeV higgsino region, and the stau-coannihilation region. Finally, a roundish 68% and 95% credibility region at -3 TeV $\lesssim A_0 \lesssim 2$ TeV and large $\tan \beta$ is the A -resonance region.

The most striking difference with the results of [16] is that now the favored A_0 range is much reduced, from a maximum span of approximately 28–30 TeV, covering almost the full parameter space, to the present span of about 10 TeV, centered around zero. By comparing the solid contours in color with the previous ones in dashed lines, one can see that the two modes that were previously predominant at large $|A_0|$ in the ~ 1 TeV higgsino region are not as favored in the present scan and do not appear at 95% credibility. This is because in [16] one needed solutions with larger M_{SUSY} to fit the Higgs mass measurement. When

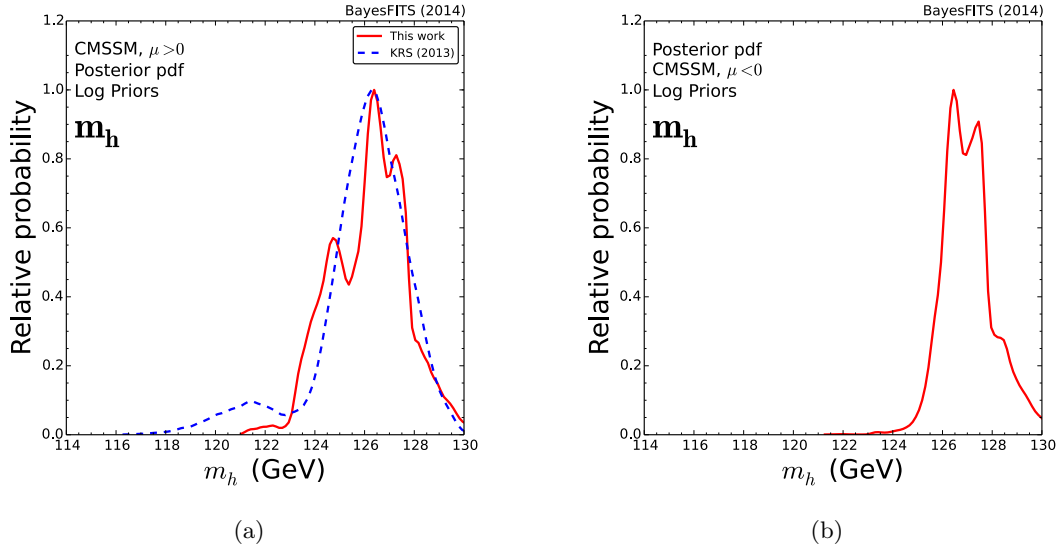


Figure 4: Marginalized 1D pdf of m_h for the CMSSM with (a) $\mu > 0$ and (b) $\mu < 0$. Red solid lines is this work, blue dashed line represents the distribution obtained in KRS 2013.

m_0 becomes very large, electroweak-symmetry breaking (EWSB) can only be obtained with large trilinear couplings, which enhance the RGE running of $m_{H_u}^2$. However, as we said above, the correct value of the Higgs mass can now be obtained with an M_{SUSY} on average smaller, even in the ~ 1 TeV higgsino region. Thus, the scanning program can more naturally find solutions with a reduced $|A_0|$.

In Fig. 3(c) we show the 68% and 95% credible regions of the 2D pdf in the $(m_0, m_{1/2})$ plane of the CMSSM for $\mu < 0$. Two of the modes of the posterior are the same as in the $\mu > 0$ case, with the exception of the A -resonance region, which does not appear for negative μ because the conditions for EWSB are not met there.³ In Fig. 3(d) we show the corresponding 2D pdf in the $(A_0, \tan \beta)$ plane.

In Fig. 4(a) we show in solid red the marginalized 1D posterior distribution for the lightest Higgs mass. We also show with a dashed blue line the distribution obtained in [16], to facilitate comparison. The posterior is in good agreement with the previous study, in which the Higgs-mass likelihood was a simple gaussian function centered about the measured CMS value, with experimental and theoretical uncertainties added in quadrature. The present likelihood function is instead determined by the sum of the χ^2 contributions of the individual Higgs searches, encoded in the **HiggsSignals** program. Note that the two

³To be precise, the A -resonance region is absent not because it is disfavored by any particular constraint, but because at large $\tan \beta$ **SoftSusy** easily incurs negative values of the \overline{DR} pseudoscalar mass squared, $m_A^2(\overline{DR})$, during the iterative procedure of RGE running. The matter was solved in earlier versions of the program by switching to the pole mass at each iteration while looking for convergence. It is debatable whether such a solution is enough to produce the correct EWSB. Thus, following the default setting in recent versions of **SoftSusy**, we have decided not to include the points of the A -resonance region for $\mu < 0$. We also abstain from showing a direct comparison with the results of [16] in this case, as they were obtained with an earlier modified version of **SoftSusy**.

main peaks in the distribution, characteristic of the A -resonance region about 124–125 GeV, and of the ~ 1 TeV higgsino region for larger m_h , are now much more in agreement with each other than in the previous study. This is the effect of including the higher order Higgs corrections: there are virtually no regions left in the parameter space for which constraints other than the Higgs searches push the posterior distribution toward $m_h < 123$ GeV.

The equivalent distribution for the case with $\mu < 0$ is shown in Fig. 4(b). In Fig. 5 we show the marginalized 1D posteriors for the heavy Higgs bosons and a selection of superpartner masses for $\mu > 0$. Again, the dashed blue line in the figures shows the distribution for the scan of Ref. [16].

In Fig. 5(a) we show the pdf for the mass of the lightest neutralino. The posterior presents three main modes, corresponding to the regions defined in Fig. 3(a). From the left to the right one can see: the stau-coannihilation region, with $0.3 \text{ TeV} \lesssim m_\chi \lesssim 0.6 \text{ TeV}$, subtending approximately 1% of the total probability; the A -resonance region, $0.6 \text{ TeV} \lesssim m_\chi \lesssim 0.9 \text{ TeV}$, with a probability of $\sim 30\%$; and the ~ 1 TeV higgsino region for $m_\chi \gtrsim 0.9 \text{ TeV}$, with $\sim 69\%$ probability. The inclusion of higher order corrections to the Higgs mass has caused the shift of a substantial fraction of posterior probability to the A -resonance region. As the dashed blue line shows, the ~ 1 TeV higgsino region was strongly favored in [16], featuring $\sim 94\%$ of the total probability, while the remainder was split in approximately equal parts between the other two regions. Note also that the average m_χ in the ~ 1 TeV higgsino region is slightly larger than in [16], as the PLANCK-measured value of the relic density is a little larger than the one measured by WMAP [96].

The 1D pdf for the heavy Higgs masses is shown in Fig. 5(b). As could be expected, the distribution features a sharp peak in the A -resonance region, for $m_A \approx 2m_\chi \lesssim 2.5 \text{ TeV}$. The ~ 1 TeV higgsino region is instead characterized by a much broader range of values, extending up to $\sim 15 \text{ TeV}$. We will show below that a large fraction of the A -resonance regions is within the reach of Higgs searches at the LHC 14 TeV run.

The 1D posterior distributions for the mass of the lightest stop, $m_{\tilde{t}_1}$, and that of the left-handed first and second generation squarks, generically indicated with $m_{\tilde{u}_L}$, are shown in Figs. 5(c) and 5(d), respectively. While the lightest squark masses in the figures, typical of the stau-coannihilation region, are now disfavored by the present limits from direct SUSY searches at the LHC, the increased relevance of the A -resonance region, which features in general lighter squarks than the ~ 1 TeV higgsino region, leads to a moderate optimism for squark detection in future-generation colliders. In particular, by comparing the solid red and dashed blue lines in, e.g., Figs. 5(c) and 5(a), one can see that in [16] there was a $\sim 30\%$ of probability favoring $m_{\tilde{t}_1} \gtrsim 8 \text{ TeV}$ (with $m_\chi \gtrsim 1 \text{ TeV}$) that has now been virtually erased. On the other hand, the parameter space featuring $m_{\tilde{t}_1} \lesssim 4 \text{ TeV}$ (with $m_\chi \lesssim 0.8 \text{ TeV}$) is now favored by roughly the same odds.

Equivalently, one can see in Fig. 5(e), where we show the 1D pdf for the gluino mass $m_{\tilde{g}}$, that the increased relevance of the A -resonance region leads to the emergence of a new peak in probability at $m_{\tilde{g}} \simeq 3 - 4 \text{ TeV}$.

Finally, we show in Fig. 5(f) the 1D posterior for the lightest chargino mass, $m_{\chi_1^\pm}$. The bulk of the probability is subtended by the ~ 1 TeV higgsino region, in which the lightest chargino is also higgsino-like and almost degenerate with the neutralino, in the

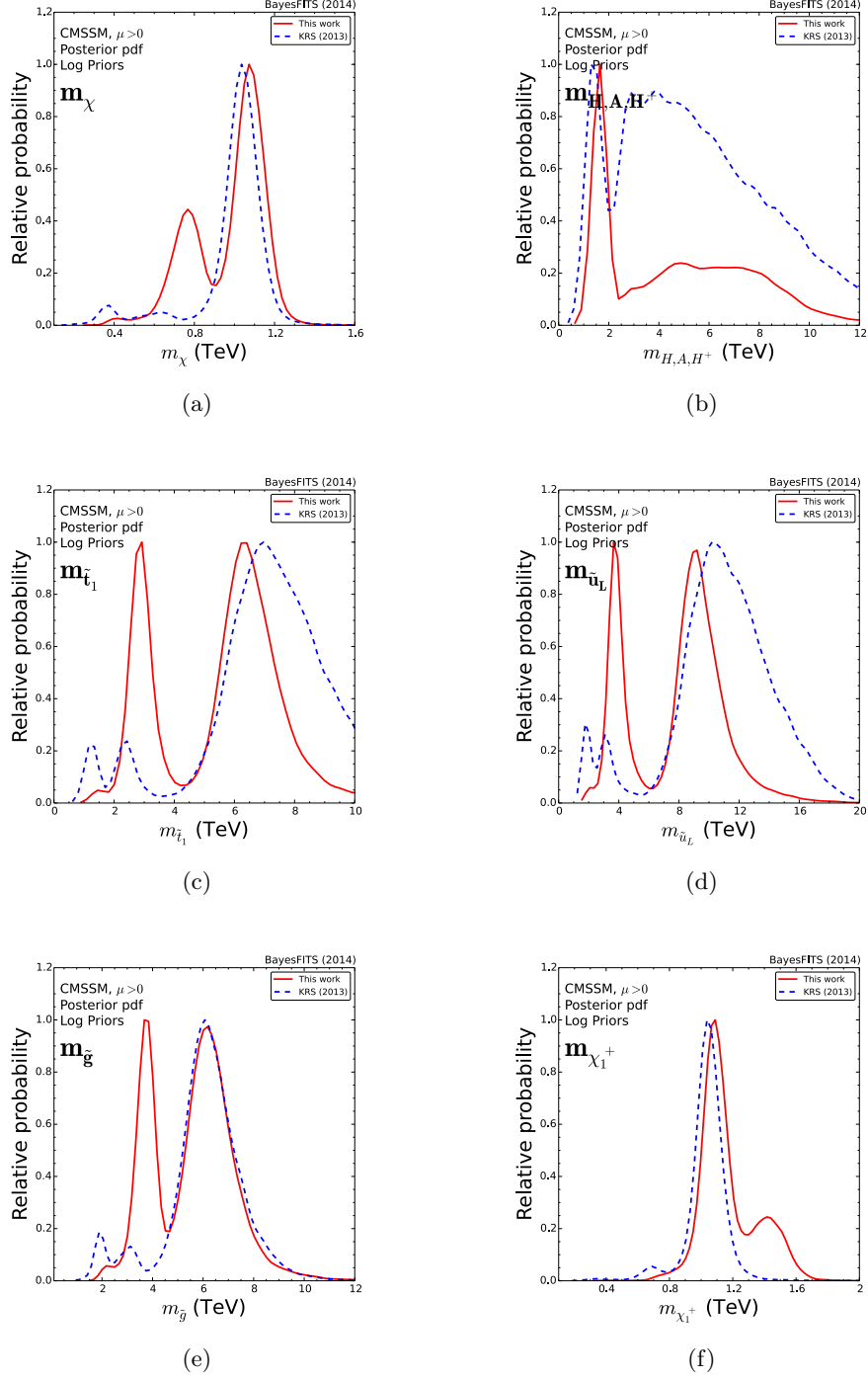


Figure 5: Marginalized 1D pdf for the heavy Higgs bosons and a selection of superpartner masses in the CMSSM with $\mu > 0$. Red solid line is this work, blue dashed lines represent distributions obtained in KRS 2013.

range $0.9 \text{ TeV} \lesssim m_{\chi_1^\pm} \lesssim 1.3 \text{ TeV}$. To the left and to the right of this larger mode, one can see the modes for the stau-coannihilation and A -resonance region, respectively. In both of

them, the neutralino is bino-like, the chargino wino-like, and one finds $m_{\chi_1^\pm} \approx 2m_\chi$.

An ATLAS study [97] of the sensitivity reach for direct SUSY searches at the LHC 14 TeV run showed that the chances of probing in this way squark masses typical of the A -resonance region are scant, to say the least. For example, with 3000 fb^{-1} of integrated luminosity, 0- and 1-lepton searches for third generation squarks have the potential, when combined, to exclude at the 95% C.L. simplified models with stop next-to-LSP (NLSP) up to $m_{\tilde{t}_1} \simeq 1.4 - 1.5 \text{ TeV}$ for $m_\chi \lesssim 0.6 \text{ TeV}$. However, it was shown in [98] that if the same luminosity were obtained at a future 33 TeV proton collider, one could exclude at the 95% C.L. simplified models with gluino NLSP up to $m_{\tilde{g}} \simeq 5 \text{ TeV}$ for $m_\chi \lesssim 2 \text{ TeV}$, or first-two generation squark NLSP up to $m_{\tilde{u}_L} \simeq 3.5 \text{ TeV}$ for $m_\chi \lesssim 1 \text{ TeV}$.

The reach for the CMSSM is going to be reduced with respect to the simplified models, due to complex decay chains that include intermediate charginos and neutralinos. Nevertheless, the same paper [98] also showed that 3000 fb^{-1} in a 100 TeV machine can extend the sensitivity for gluino NLSP to $m_{\tilde{g}} \simeq 12 \text{ TeV}$ for $m_\chi \lesssim 4 \text{ TeV}$, or first-two generation squark NLSP up to $m_{\tilde{u}_L} \simeq 8 \text{ TeV}$ for $m_\chi \lesssim 2 \text{ TeV}$.

Obviously, it seems that the $\sim 1 \text{ TeV}$ higgsino region of the CMSSM remains for the most part beyond the direct reach of conceivable future colliders. Note, however, that it was shown in [33] that this is not necessarily the case when the assumptions of GUT-scale universality are relaxed.

For $\mu < 0$ the 1D distributions of particle masses share identical features with the positive μ case with the exception that the peaks associated with the A -resonance region described above are absent. Since this generally leaves only posterior probability in the region of large superpartner masses far beyond the reach of the LHC we do not show these distributions.

In Fig. 6(a) we show the marginalized 2D pdf projected to the $(m_A, \tan\beta)$ plane. In the A -resonance region, characterized by $m_A < 2.5 \text{ TeV}$ and $\tan\beta > 45$, the posterior appears to be well localized. In the CMSSM, this limited range of m_A and $\tan\beta$ values is a proper feature of the A -resonance region, as was extensively explained in [16], namely large $\tan\beta$ value and neutralino not excessively heavy must conspire to produce a region of resonance, $m_A \approx 2m_\chi$, and a cross section large enough to yield the relic density measured at PLANCK. One can see that m_A and $\tan\beta$ are not as tightly constrained for the two remaining modes, so that the posterior spreads over a broad range of values. In particular, the stau-coannihilation region is localized in m_A , $m_A \simeq 1.5 - 2 \text{ TeV}$, but not in $\tan\beta$; the $\sim 1 \text{ TeV}$ higgsino region covers instead the majority of the parameter space with $m_A \gtrsim 2.5 \text{ TeV}$, $\tan\beta \gtrsim 5$. To make this feature more visible we superimposed in the figure a sample of points drawn from the posterior distribution.

It was shown in [16] that, since the points of the A -resonance region are well localized in the $(m_A, \tan\beta)$ plane, the whole region can be easily tested through precise measurement of $\text{BR}(B_s \rightarrow \mu^+ \mu^-)$, which is proportional to $\tan^6 \beta / m_A^4$. Here, we show that the same features also make a large fraction of the points testable at the LHC through Higgs searches in the $\tau^+ \tau^-$ channel.

In Fig. 6(b) we show a zoomed-in fraction of the $(m_A, \tan\beta)$ plane. The limits from direct $A \rightarrow \tau^+ \tau^-$ searches at CMS with $\sim 17 \text{ fb}^{-1}$ [100] are included in HiggsBounds. In

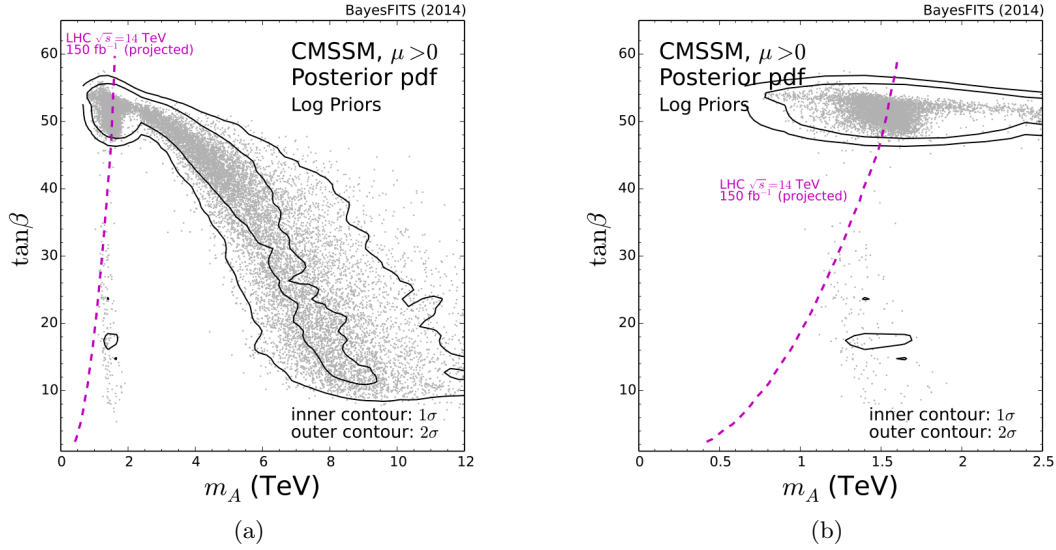


Figure 6: (a) Marginalized 2D posterior distribution for the CMSSM with $\mu > 0$ in the $(m_A, \tan \beta)$ plane. (b) A zoomed-in fraction of the same. The inner contours give the 68% credible regions and the outer ones the 95% credible regions. A sample of points (in gray) drawn from the posterior distribution is shown for clarity. The magenta dashed lines show the expected reach at LHC 14 TeV with $\sim 150 \text{ fb}^{-1}$ estimated in [99].

the M_h^{max} scenario [101], they exclude m_A up to approximately 800 GeV for $\tan \beta \simeq 50$. However, it was explained in [102] that they are robust against radiative corrections to the MSSM Higgs, and can be considered almost scenario-independent. Ref. [99] estimated the sensitivity reach of the LHC 14 TeV run with $\sim 150 \text{ fb}^{-1}$ in the $\tau^+\tau^-$ channel for the heavy MSSM Higgs bosons. We show the expected 95% C.L. reach as a magenta dashed line in Figs. 6(a) and 6(b). Approximately 50% of the points in the A -resonance region fall within the expected sensitivity.

3.2 Prospects for dark matter detection

In Fig. 7(a) we show the 2D posterior distribution in the $(m_\chi, \sigma_p^{\text{SI}})$ plane for $\mu > 0$. The different regions are well separated and can be identified from left to right as the stau-coannihilation, A -resonance and $\sim 1 \text{ TeV}$ higgsino regions. We show the current best upper limit from LUX 90% C.L. as a red solid line, the previous one from XENON100 as a gray dot-dashed line, and the projected sensitivity of XENON-1T [103] as a magenta dashed line. The bino-like neutralino typical of the stau-coannihilation and A -resonance regions has a suppressed coupling to the nucleus, so that both regions lie well below the current LUX bound and it is very unlikely they will be tested, even with the improved sensitivity of XENON-1T. In contrast, the $\sim 1 \text{ TeV}$ higgsino region lies almost entirely within the projected XENON-1T sensitivity. The entire 68% and nearly all of the 95% credibility region have the potential to be probed in the next few years, encompassing about 70% of the points in the scan. This makes dark matter direct detection searches the predominant

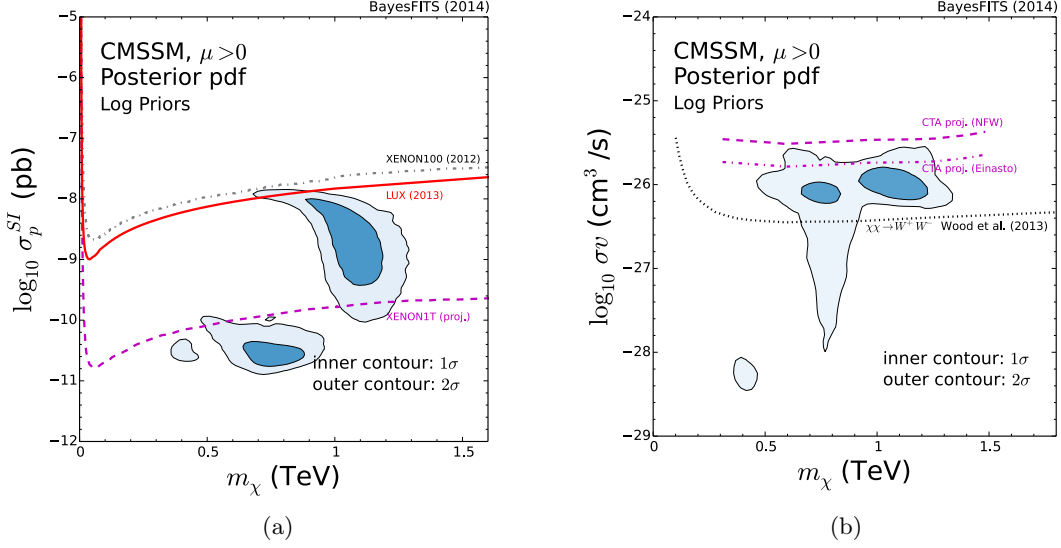


Figure 7: (a) Marginalized 2D posterior distribution for the CMSSM with $\mu > 0$ in the $(m_\chi, \sigma_p^{\text{SI}})$ plane. The red solid line shows the 90% C.L. upper bound as given by LUX, here included in the likelihood function. The gray dot-dashed line shows the 2012 XENON100 90% C.L. bound [70] and the magenta dashed line shows projected sensitivity for 2017 at XENON-1T [103]. (b) Marginalized 2D posterior distribution for the CMSSM with $\mu > 0$ in the $(m_\chi, \sigma v)$ plane. The magenta dashed line shows the expected sensitivity of CTA under the assumptions of [36] for a NFW halo profile. The magenta dot-dashed line shows the corresponding sensitivity with Einasto profile. The dotted black line shows the projected sensitivity of the CTA expansion considered in [104].

tool for exploration of the CMSSM.

In the CMSSM the largest cross section values, $\sigma_p^{\text{SI}} \gtrsim 10^{-8}$ pb, are obtained in the focus point region. One can see the beginning of the horizontal branch joining the higgsino and focus point regions, at $m_\chi \simeq 0.7 - 0.8$ TeV. The effect of the LUX limit in the likelihood is visible, as the credibility region is cut off rapidly after crossing the 90% C.L. bound, shown in red. In contrast to [16], this causes the focus point region to be disfavored by the scan. In the $\mu < 0$ scenario we obtain the same results albeit with the absence of the A -resonance region. The sign of the μ parameter has little impact on σ_p^{SI} for the neutralino and the ~ 1 TeV higgsino region with $\mu < 0$ can also be entirely probed by XENON-1T.

In Fig. 7(b) we show the 2D posterior distribution in the $(m_\chi, \sigma v)$ plane. The node at $\sigma v \lesssim 10^{-28}$ cm³/s is the stau-coannihilation region, which has a much reduced σv in the present day due to the absence of co-annihilations with the stau NLSP, which are instead only present in the early Universe. The A -resonance and ~ 1 TeV higgsino regions are visible at larger σv , from left to right, respectively. The A -resonance region is characterized by a broad range of cross section values, with a deep funnel at 95% credibility that extends down to $\sigma v \simeq 10^{-28}$ cm³/s. This corresponds to a large resonant effect in the early Universe when the neutralinos are distributed thermally, but the present value of σv is small since the colliding neutralinos have insufficient energy to produce the pseudoscalar on shell (see, e.g., Appendix B in [31]). σv is reduced by orders of magnitude in this funnel and is

effectively impossible to probe via indirect detection.

As was the case for direct detection, the ~ 1 TeV higgsino region presents a particularly promising target for indirect detection since the annihilation cross section is restricted to a small range close to the thermal value compared to other dark matter candidates in the MSSM which can have much lower annihilation cross sections. The magenta dashed and dot-dashed lines in Fig. 7(b) show the expected sensitivity of CTA derived in Sec. 2 under the assumptions of the NFW [105] and Einasto [106] halo profile, respectively. The dotted line shows the projected sensitivity of CTA to the W^+W^- final state, as obtained in Ref. [104] under a more optimistic setup including more telescopes in the array. As previously discussed, limits on single final states may not automatically exclude all points in the posterior since the neutralino will usually annihilate into several different final states depending on its mass and composition. The W^+W^- final state does however provide a good approximation in the ~ 1 TeV higgsino region and points in this region lying above the W^+W^- line have the potential to be constrained. We note that current limits from the Cherenkov telescope array HESS [83] are approximately an order of magnitude larger than the projected CTA sensitivity and so do not constrain the posterior regions found.

One can see that the derived CTA limits lie just above the 68% credibility posterior region for either choice of dark matter profile, but significant improvements to the limits are possible by improving the experimental setup. It should be noted that a factor of five improvement in the model independent limit on the number of observed gamma rays would be sensitive to the entire ~ 1 TeV higgsino region and to the bulk of the A -resonance region, thus the vast majority of the favored points in the CMSSM.

The higgsino and stau-coannihilation regions in the negative μ case share the same properties as the positive μ case and have the same prospects for detection, we therefore do not show their distribution here.

4 Results in the NUHM

4.1 Posterior distributions and prospects for collider searches

We proceed now to the analysis of the NUHM. The parameters m_0 , $m_{1/2}$, A_0 , and $\tan\beta$ were scanned in the same ranges as in the CMSSM. The parameters $m_{H_d}^2$ and $m_{H_u}^2$ were allowed to assume negative values at the GUT scale; see Table 2. We limit ourselves to the case with $\mu > 0$, which, as was seen for the CMSSM, presents a greater number of solutions. One must keep in mind that the solutions with $\mu < 0$ can generally be mapped to a subset of the ones we present in here, without novel phenomenological features.

In Fig. 8(a) we show the marginalized 2D posterior in the $(m_0, m_{1/2})$ plane. The 68% and 95% credible regions are indicated by inner and outer solid contours, respectively. In this and the following figures we superimpose on the clearly marked credible regions a set of points drawn from the posterior distribution. We include those points since, unlike in the CMSSM, the points that satisfy the relic density constraint are not always found in regions of parameter space well separated along different mechanisms of neutralino annihilation. Thus, the distribution and position of the points in the plots highlight details not always

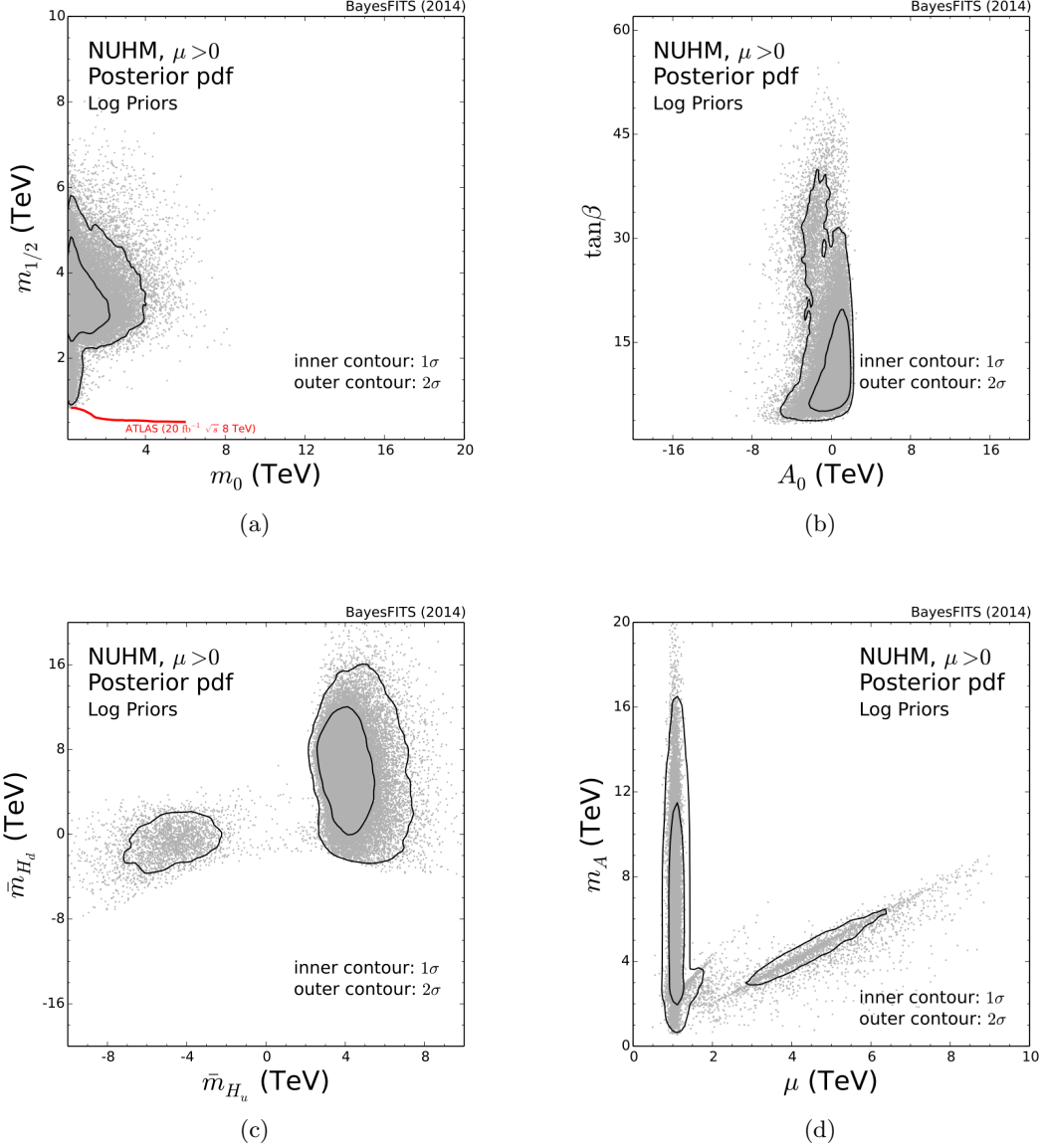


Figure 8: Marginalized 2D posterior in (a) the $(m_0, m_{1/2})$, (b) the $(A_0, \tan\beta)$, (c) the $(\tilde{m}_{H_u}, \tilde{m}_{H_d})$, and (d) the (μ, m_A) planes of the NUHM with $\mu > 0$. 68% and 95% credible regions are shown by the inner and outer contours, respectively. Gray points are distributed according to the posterior probability. The ATLAS 95% C.L. exclusion line is shown in red solid for reference.

easy to infer from the contours and help indicate where additional solutions beyond the 95% credibility regions can be found.

The mechanisms to reduce the relic density are for the most part in common with the CMSSM: stau co-annihilation and A -resonance of bino-like neutralinos, and annihilation and co-annihilation of ~ 1 TeV higgsino-like neutralinos and charginos. We shall see, though, that the NUHM also presents some additional ways of obtaining the correct relic density. Moreover, all of those mechanisms can be obtained for m_0 not too large, in contrast

with the ~ 1 TeV higgsino region of the CMSSM, thanks to the additional freedom in the Higgs sector. Thus the posterior shows a more compact shape in $(m_0, m_{1/2})$ plane, due also to the effect of log prior distributions. Had we used flat priors, volume effects would inflate the region of large m_0 and $m_{1/2}$ and therefore increase the importance of the ~ 1 TeV higgsino region in the NUHM.

The marginalized posterior in the $(A_0, \tan \beta)$ plane is shown in Fig. 8(b). As was the case for the CMSSM, the solutions tend to be distributed over the entire $\tan \beta$ range, but now favor relatively smaller values of $|A_0|$ than in previous scans.

In Fig. 8(c) we show the marginalized 2D pdf in the $(\bar{m}_{H_u}, \bar{m}_{H_d})$ plane.⁴ One can see here a previously unexplored 95% credibility region featuring negative values for \bar{m}_{H_u} at the GUT scale and, for the majority of the points involved, also $\bar{m}_{H_d} < 0$.

Large negative values of $m_{H_u}^2$ at the GUT scale lead to large negative value for the same parameter at M_{SUSY} . Through the EWSB condition, these points thus feature very large values of μ , up to ranges previously unexplored in NUHM analyses. We show the marginalized 2D pdf in the (μ, m_A) plane in Fig. 8(d). The described solutions can be seen on the lower right end of the plot, for values of μ that can be as large as 9 TeV.⁵

The correct relic density for these points is obtained through mechanisms of stau-coannihilation. In fact, values of μ so large strongly enhance the coupling of the lightest stau to the H_u component of the lightest Higgs, thus increasing the efficiency of the annihilation channel $\tilde{\tau}\tilde{\tau} \rightarrow hh$. The $\tilde{\tau}\tilde{\tau}h$ vertex, proportional to μ , leads to a μ^4 enhancement of the annihilation cross section, which becomes the dominant mechanism when the lightest stau and neutralino are almost degenerate in mass. We show in Fig. 9(a) the 2D pdf in the $(m_\chi, m_{\tilde{\tau}_1})$ plane. One can see that because of the above considerations, stau-coannihilation in the NUHM is efficient up to $m_\chi \simeq 2$ TeV, thus significantly extending the range observed in the CMSSM, or in previous studies performed with more limited ranges of μ [11, 14].

Figures 8(c) and 8(d) show that the vast majority of the points with high posterior probability feature, at the GUT scale, positive values of $m_{H_u}^2$ and $m_{H_d}^2$, and at the weak scale, $\mu \simeq 1$ TeV. Thus, as was the case for the CMSSM, in the NUHM the largest number of solutions belong to the ~ 1 TeV higgsino region. The predominance of this region was also shown in Ref. [14], where it was the *only* region found, due to their choice of input parameters and prior ranges. The extended stau-coannihilation region shown in Figs. 8 and 9 is instead a novel finding of this study.

Moreover, as was mentioned at the beginning of this section, in the NUHM there are also a significant number of solutions for which the neutralino annihilates via the resonance with heavy Higgs bosons, as already pointed out in [16, 30]. We show in Fig. 9(b) the 2D pdf in the (m_χ, m_A) plane, which shows the presence of many points at $m_A \approx 2m_\chi$. Those points cannot be identified as easily in other plots: for example, in Fig. 8(c) they are shown

⁴Here \bar{m}_{H_u} and \bar{m}_{H_d} refer to the signed square root of the absolute value of $m_{H_u}^2$ and $m_{H_d}^2$, respectively. E.g., $\bar{m}_{H_u} = m_{H_u}^2 / \sqrt{|m_{H_u}^2|}$.

⁵It is clear that these solutions present uncomfortably large values of EW fine tuning due the large μ parameter, so that they might be unappealing from a theoretical point of view. However, in this paper we are only concerned with the existence of viable phenomenological solutions, independently of theoretical considerations. We will therefore treat these solutions without further mentioning the fine-tuning issue.

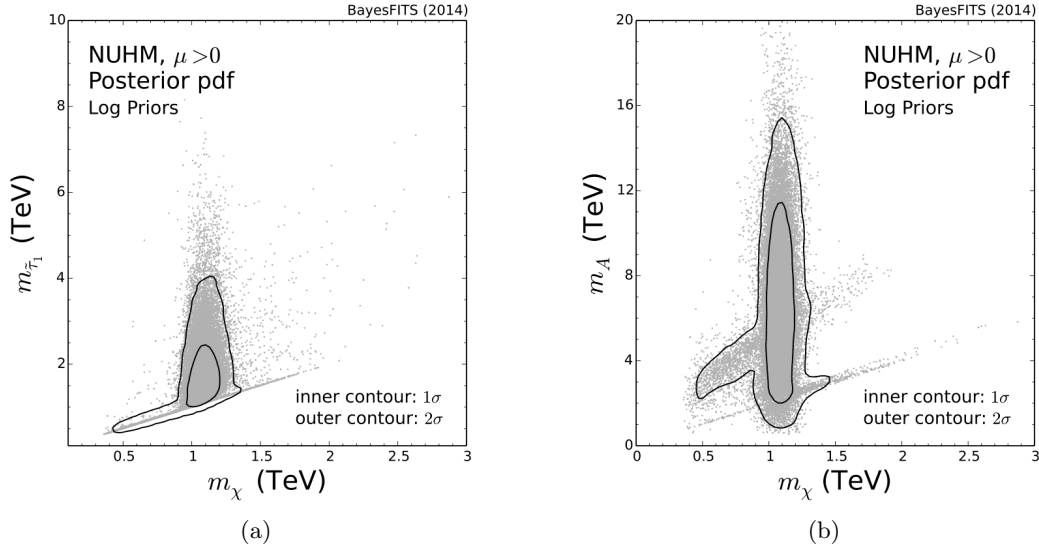


Figure 9: Marginalized 2D posterior in (a) the $(m_\chi, m_{\tilde{\tau}_1})$ plane and (b) the (m_χ, m_A) plane of the NUHM with $\mu > 0$. 68% and 95% credible regions are shown by the inner and outer contours, respectively. Gray points are distributed according to the posterior probability.

as diffuse points lying between the two high posterior probability modes described above, and as a subset of points in the right hand mode restricted to $\tilde{m}_{H_d} < 4$ TeV (above this value $m_{H_d}^2$ drives m_A to be too large to find solutions with $m_A \approx 2m_\chi$). We point out here that, while in the CMSSM the points of the A -resonance region feature neutralinos with very large bino composition, and very large $\tan\beta$ values, this is not always the case in the NUHM. Thus, while in the CMSSM the main annihilation channel for those points is $\chi\chi \rightarrow b\bar{b}$, many of the A -resonance points with $m_\chi > 1.2$ TeV in Fig. 9(b) feature much larger higgsino fraction and moderate $\tan\beta$ values, so that the correct relic density is obtained in a combined fashion: with $t\bar{t}$ final states in addition to $b\bar{b}$, and through resonance with the heavy scalar H , degenerate with A , in addition to the pseudoscalar. As we shall see in Sec. 4.2 this fact has important consequences for dark matter direct detection.

Figure 9(b) neatly shows the different annihilation mechanisms described above: the large concentration of points at $m_\chi \simeq 1$ TeV gives the ~ 1 TeV higgsino region; at $m_A \approx 2m_\chi$ there is the strip of points belonging to the just-described A/H -resonance region, which induces a lobe in the 95% credible region of the posterior for $m_\chi \gtrsim 1.2$ TeV; and, finally, the stau-coannihilation region, which produces a lobe in the posterior with $m_\chi \lesssim 1$ TeV, but can in fact extend up to $m_\chi \lesssim 2$ TeV.

We show in Fig. 10 the 1D pdf distribution of the lightest Higgs mass, m_h . The black dot-dashed line shows the distribution obtained for the CMSSM with $\mu > 0$ for comparison. One can see that the posterior is prevalently uni-modal due to the statistical dominance of the ~ 1 TeV higgsino region in the NUHM.

In Fig. 11 we present the marginalized 1D posterior distributions for the heavy Higgs bosons and a selection of superpartner masses. As a comparison we show the correspond-

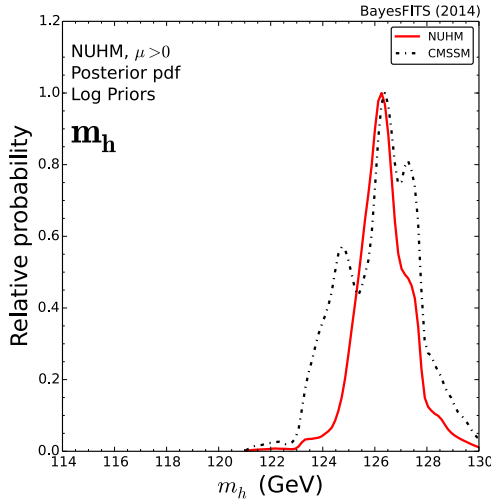


Figure 10: Marginalized 1D pdf of m_h for the NUHM with $\mu > 0$. The black dot-dashed line shows the distribution obtained for the CMSSM with $\mu > 0$ for comparison.

ing CMSSM distributions from Fig. 5 as black dot-dashed lines. Figure 11(a) shows the distribution for m_χ . One can see one single peak at $m_\chi \simeq 1$ TeV, indicating that in the NUHM the ~ 1 TeV higgsino region dominates the posterior probability, with the other two regions significantly less favored and spread over a broad range of m_χ values.

In Fig. 11(b) we show the distribution of the heavy Higgs masses. As mentioned above, the A/H -resonance region extends over a large range of m_A values, and the posterior probability associated with it is much reduced relative to the CMSSM. As a consequence, values of $m_A > 2-3$ TeV, typical of the ~ 1 TeV higgsino region, are instead favored in the NUHM, thus making the prospects for sensitivity at the LHC ($A \rightarrow \tau^+\tau^-$ direct searches) much bleaker than in the CMSSM.

Analogous conclusions pertain to the prospects for LHC observation of the other SUSY particles. In Figs. 11(c) and 11(d) we show the distributions for the lightest stop mass and squark masses for the first two generations, respectively. In Fig. 11(e) we show the distribution for the gluino mass. The bulk of the squark mass distributions are peaked around mass values significantly smaller than in the corresponding ~ 1 TeV higgsino region of the CMSSM, as the posterior does not extend as much in m_0 , but they are still well outside the most optimistic reach for direct detection at the LHC.

One observes some solutions in common with the CMSSM, in the stau-coannihilation region, characterized by $m_{\tilde{t}_1} \lesssim 1.5$ TeV, $m_{\tilde{u}_L} \lesssim 3$ TeV, or $m_{\tilde{g}} \lesssim 3$ TeV, and a neutralino that can be as light as 0.4 TeV. Those might begin to be probed at the 14 TeV run of the LHC. However, as was explained above, the stau-coannihilation region in the NUHM extends significantly with respect to the CMSSM, reaching quite large $m_{1/2}$ values. Thus, it favors heavier gluinos, neutralinos, and scalars, and the statistical weight of the parameter space in reach of the LHC is much reduced.

Finally, we show for completeness in Fig. 11(f) the 1D pdf for the lightest chargino.

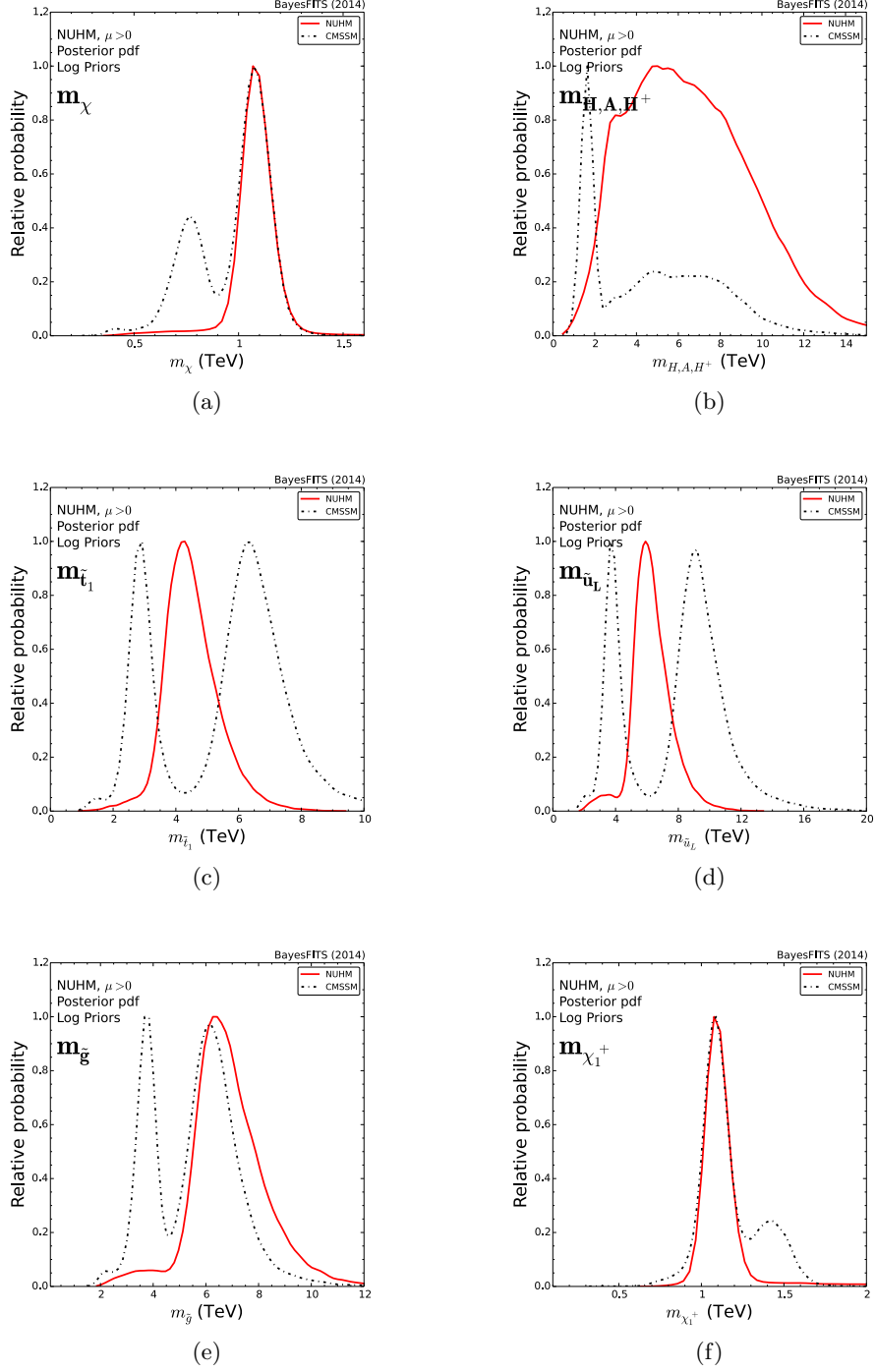


Figure 11: Marginalized 1D pdf for the heavy Higgs bosons and a selection of superpartner masses in the NUHM with $\mu > 0$. Black dot-dashed lines are the distributions obtained for the CMSSM with $\mu > 0$ for comparison.

One can see the predominant peak at $m_{\chi_1^\pm} \simeq 1$ TeV, encompassing models with higgsino-

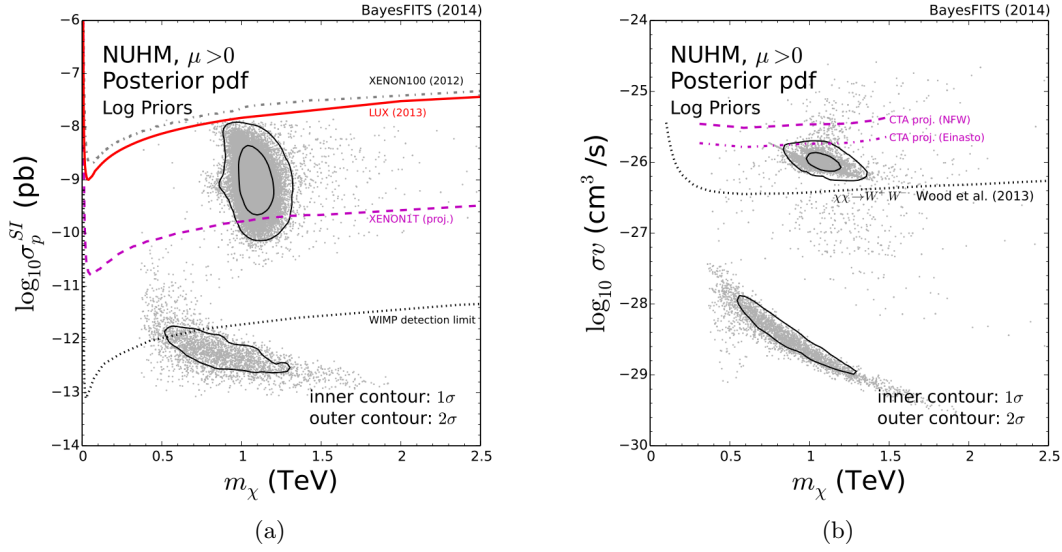


Figure 12: (a) Marginalized 2D posterior distribution in the (m_χ, σ_p^{SI}) plane of the NUHM with $\mu > 0$. The solid red line shows the 90% C.L. upper bound as given by LUX, here included in the likelihood function. The dot-dashed gray line shows the 90% C.L. 2012 bound of XENON100. The projected sensitivity for 2017 at XENON-1T is shown in magenta dashed. The black dotted line marks the onset of the irreducible neutrino background. (b) Marginalized 2D posterior distribution for the NUHM with $\mu > 0$ in the $(m_\chi, \sigma v)$ plane. The magenta dashed line shows the expected sensitivity of CTA under the assumption of a NFW halo profile. The magenta dot-dashed line shows the corresponding sensitivity with Einasto profile. The thin dotted line shows the projected sensitivity of the CTA expansion [104].

like χ_1^\pm , accompanied by a lower tail that extends to larger mass values, typical of the wino-dominated charginos.

4.2 Prospects for dark matter detection

In Fig. 12(a) we show the marginalized 2D posterior distribution in the (m_χ, σ_p^{SI}) plane. As was the case in the CMSSM, shown in Fig. 7(a), one can easily identify the ~ 1 TeV higgsino region as the large 68% and 95% credible region at $m_\chi \simeq 1 - 1.2$ TeV right below the LUX limit.

The characteristics of this region are largely independent of the model, so that the prospects for detection are similar to the CMSSM. However, the relative probability of this region is larger in the NUHM, being greater than 90%, versus approximately 70% of the total probability in the same region of the CMSSM.

On top of this, as was mentioned when discussing Fig. 9(b), many of the solutions in the A/H -resonance region of the NUHM feature mixed composition, bino-higgsino neutralinos with $m_\chi \gtrsim 1.2$ TeV, with consequently enhanced couplings to the nucleus. Those points can be seen in Fig. 12(a) scattered below the LUX limit, well in reach of the XENON-1T sensitivity, shown with a magenta dashed line,

On the negative side, one can see that the remaining 95% credible region, the stau-coannihilation region, now extends to much smaller values of σ_p^{SI} and for neutralinos heavier

than $m_\chi \simeq 0.8 \text{ TeV}$ it lies below the onset of irreducible neutrino background [107, 108] calculated in [109], shown with a black dotted line. For σ_p^{SI} below the black dotted line the background of atmospheric and diffuse supernova neutrinos becomes important, so that the sensitivity scales with square root of exposure, making the neutralino more difficult to detect via direct detection experiments.

Finally, we show in Fig. 12(b) 2D posterior distribution in the $(m_\chi, \sigma v)$ plane. As was explained in Sec. 2 the estimated CTA sensitivity is indicatively shown for the NFW and Einasto halo profile as a magenta dashed and dot-dashed line, respectively. One must remember that the sensitivity of the individual points in the scan strongly depends on the annihilation final states, so that the lines in Fig. 12(b) must be taken with care. However, the indicated sensitivity is robust for final states characterized by gauge bosons, which are very typical of the $\sim 1 \text{ TeV}$ higgsino region, shown in the figure as the predominant 68% and 95% posterior region.

Thus, one can extend to the NUHM the conclusion already stated for the CMSSM in Sec. 3.2. The projected sensitivity in the minimal configuration studied here⁶ seems to fall just short of biting significantly into the parameter space of the model. But extended configurations considered in the literature or, alternatively, an improvement in the estimated sensitivity, have the potential to deeply probe the bulk of the model’s parameter space, thus yielding a complementary test with respect to direct detection searches.

5 Summary and conclusions

In this paper we performed a Bayesian analysis of the CMSSM and the NUHM. We presented the 68% and 95% credible regions of the marginalized 2D posterior pdf and the 1D distributions of relevant parameters and observables in light of the latest experimental constraints and updated numerical tools.

In particular, we updated the results of our previous study [16] by *a)* including the corrections to the lightest Higgs mass beyond the 2-loop order using `FeynHiggs v2.10.0`, which calculates the leading and next-to-leading log corrections in the top/stop sector resummed at all orders in perturbation theory; *b)* including in the likelihood function the latest constraints from direct SUSY searches at the LHC with $\sim 20 \text{ fb}^{-1}$ at 8 TeV; and *c)* including in the likelihood function the most recent constraints from direct detection of dark matter at LUX.

We find that the higher-order corrections to the Higgs mass induce modifications to the posterior probability distribution with respect to [16]. The correct value of the Higgs boson mass now requires an M_{SUSY} in general lower, so that the 95% credible regions do not extend beyond $m_0 \simeq 12 \text{ TeV}$ in the CMSSM. Moreover, regions of the parameter space that in the past struggled to produce a $\sim 126 \text{ GeV}$ Higgs mass, can now do it more easily. As a consequence, we observe increased statistical relevance of the *A*-resonance region of the CMSSM relative to [16], with approximately 30% of the total probability. This improves the chances for direct observations of the pseudoscalar Higgs at the LHC 14 TeV run, in

⁶We use the setup considered in [36] called Array I consisting of 3 large size telescopes, 18 medium size telescopes and 56 small size telescopes.

the $A \rightarrow \tau^+ \tau^-$ channel. It also potentially favors direct testing in sparticle searches at future, higher-energy proton colliders.

On the other hand, the bulk of the probability still lies in the ~ 1 TeV higgsino region, comprising $\sim 70\%$ of the total in the CMSSM and $\sim 90\%$ in the NUHM. Given the almost pure higgsino nature of the dark matter candidate in this region the prospect for probing the vast majority of the parameter space of both models through dark matter detection searches is enticing.

The constraining power of future 1-tonne direct detection experiments like XENON-1T on the parameter space of the CMSSM and the NUHM has been long known, and is confirmed once more in here. In this study we also showed that indirect detection of dark matter through γ -rays from the GC at CTA is a realistic possibility in the CMSSM and the NUHM. We applied the results of Ref. [36] for the sensitivity of CTA to several annihilation final states to the case of annihilation to multiple final states, as is the MSSM. We find that the configuration studied in [36] falls just short of biting significantly into the parameter space, but a factor of 5 improvement on the sensitivity can probe $\sim 90\%$ of the favored parameter space in both models.

In summary, in both models all the regions favored by the latest constraints show good prospects for future observation. In the CMSSM, the stau-coannihilation region (1% of the total pdf) will be most likely probed in its entirety through direct SUSY searches at the LHC 14 TeV run; $\sim 50\%$ of the A -resonance region (corresponding to 15% of the total pdf) might be probed in Higgs searches at the LHC, while it was shown in [16] that the whole region is also very sensitive to improvements in the measurement of $\text{BR}(B_s \rightarrow \mu^+ \mu^-)$; the ~ 1 TeV higgsino region (70% of the pdf) will be probed via dark matter direct detection in 1-tonne experiments. Simultaneously, optimistic but not unrealistic improvements in the projected sensitivity of CTA might potentially test the whole ~ 1 TeV higgsino region and almost all of the A -resonance region.

This becomes even more important in the NUHM, where dark matter searches become the privileged instrument to probe the parameter space. In particular the largest part of the ~ 1 TeV higgsino region and a large number of A/H resonance solutions, that together cover approximately $\sim 90\%$ of the favored parameter space can be simultaneously probed at 1-tonne detectors and at CTA, if the estimated sensitivity of the latter increases as shown in this study.

ACKNOWLEDGMENTS

We would like to thank Kamila Kowalska for valuable input on the construction of the LUX likelihood. A.W. would like to thank Jamie Tattersall for email support on using **CheckMATE**. This work has been funded in part by the Welcome Programme of the Foundation for Polish Science. L.R. is also supported in part by a STFC consortium grant of Lancaster, Manchester, and Sheffield Universities. The use of the CIS computer cluster at the National Centre for Nuclear Research is gratefully acknowledged.

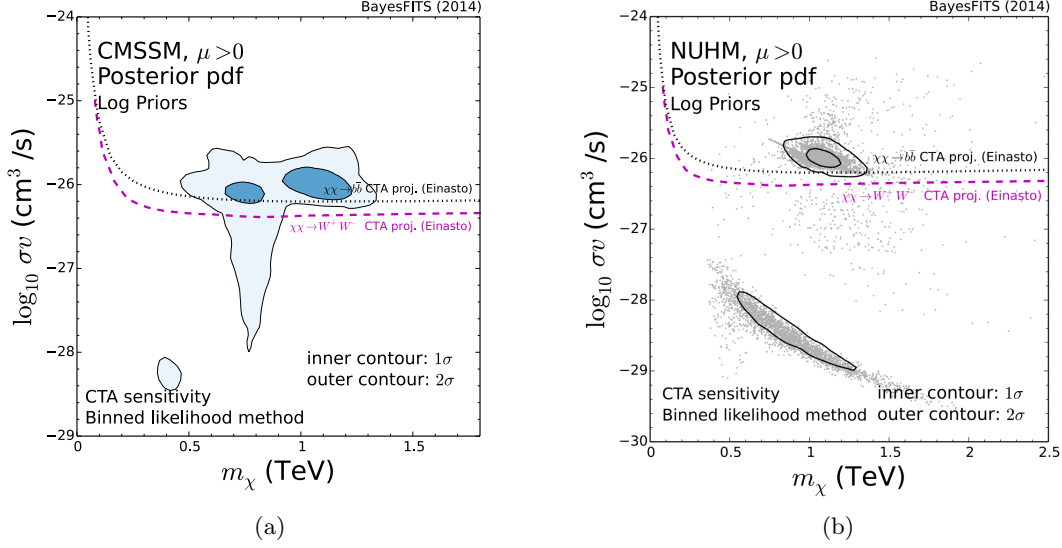


Figure 13: (a) Marginalized 2D posterior distribution for the CMSSM with $\mu > 0$ in the $(m_\chi, \sigma v)$ plane. (b) Marginalized 2D posterior distribution for the NUHM with $\mu > 0$ in the $(m_\chi, \sigma v)$ plane. In both panels the magenta dashed line shows the expected sensitivity of CTA for the W^+W^- final state under the Einasto profile assumption, calculated in Ref. [110] using the binned likelihood method. The black dotted line shows the corresponding sensitivity for the $b\bar{b}$ final state. This figure updates Figs. 7(b) and 12(b).

A Impact of a recent calculation of the sensitivity of CTA

In a recent paper [110] we calculated the projected sensitivity of CTA to the WIMP annihilation cross section, under the assumption of the Einasto or the NFW DM halo profile. We used a binned likelihood function, and the details of the calculation are presented in Appendix A of [110]. Our likelihood function leads to a higher sensitivity than the one obtained in [36], which was used in this paper to draw the projected limits shown in Figs. 2, 7(b), and 12(b). The result of our calculations for several individual final states in the MSSM, assuming the Einasto profile and 500 hours of observation, can be found in Fig. 14 of [110].

In Fig. 13(a) we show the new W^+W^- and $b\bar{b}$ projected sensitivities, obtained using the binned likelihood method, in the $(m_\chi, \sigma v)$ plane of the CMSSM. The W^+W^- final state bound provides a rough estimate of the exclusion reach for the ~ 1 TeV higgsino region, whereas the $b\bar{b}$ bound applies to the A -resonance region. In Fig. 13(b) we show the same for the NUHM. Figure 13 shows that the binned likelihood method leads to significantly improved sensitivity relative to that of Ref. [36], which was presented in Figs. 7(b) and 12(b).

In the remainder of this appendix we show that, in light of the results of [110], under reasonable assumptions the full extent of the 95% credible region of the CMSSM will be probed by a limited number of upcoming experiments. These are, by increasing mass scale:

1. CMS and ATLAS direct SUSY searches at the LHC Run II;

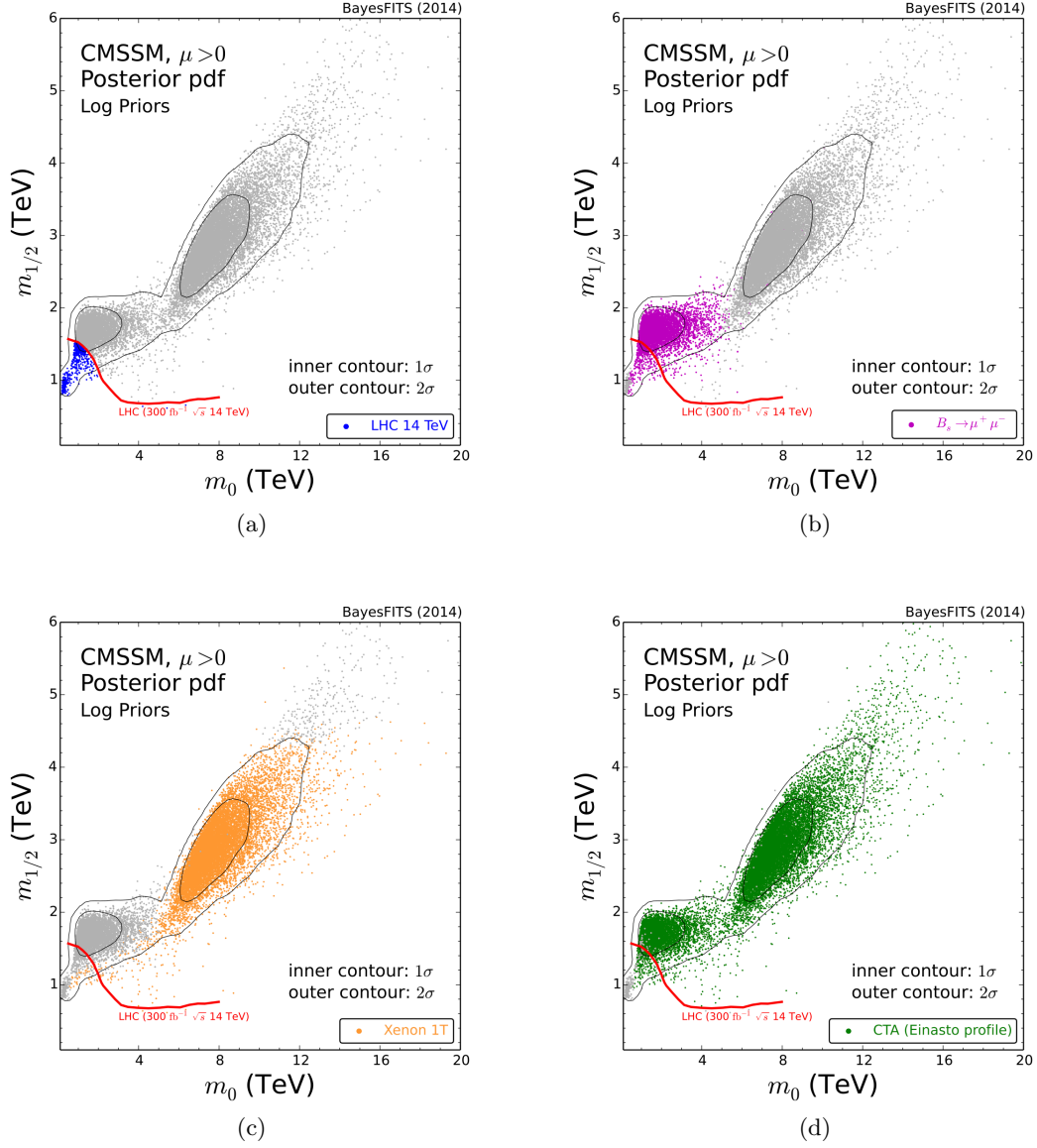


Figure 14: (a) Marginalized 2D posterior in the $(m_0, m_{1/2})$ plane of the CMSSM with $\mu > 0$. 68% and 95% credible regions are shown by the inner and outer contours, respectively. Points are distributed according to the posterior probability. The projected LHC Run II 95% C.L. exclusion line from Ref. [111] is shown in red solid for reference. Blue points lie within sensitivity for direct SUSY searches, gray points are unconstrained. (b) Same as (a) except that points in magenta are sensitive to future measurements of $\text{BR}(B_s \rightarrow \mu^+ \mu^-)$, as described in Ref. [16]. (c) Same as (a) except that points in orange lie within sensitivity of tonne-scale underground DM detectors. (d) Same as (a) except that points in green lie within sensitivity of CTA to γ rays from DM annihilations, as calculated in Ref. [110].

2. Precise measurement of $\text{BR}(B_s \rightarrow \mu^+ \mu^-)$ at LHCb in Run II;
3. Direct searches for dark matter at XENON-1T and other tonne-scale experiments;
4. Indirect detection of dark matter at CTA through γ rays from the GC.

The impact of each experiment’s projected sensitivity on the parameter space of the CMSSM is shown in the four panels of Fig. 14. In Fig. 14(a) we show a sample of points distributed according to the posterior probability, whose 68% and 95% credible regions are shown by the inner and outer contours, respectively. The points in blue lie within the projected sensitivity of searches for squarks and gluinos at the LHC Run II calculated in Ref. [111], whereas the gray points remain unconstrained. The expected limit from the 0-1 lepton + jets + missing energy searches with 300 fb^{-1} at 14 TeV is shown as a red solid line. As is well known, Run II will be sensitive to most of the remaining part of the stau-coannihilation region, presently not excluded by the LHC 8 TeV run.

As was explained in Ref. [16], one will exclude the 95% credible posterior region corresponding to the A -resonance region of the CMSSM if the measurement of $\text{BR}(B_s \rightarrow \mu^+\mu^-)$ eventually converges to its SM expectation with an error of $\sim 5\%$, and at the same time the theoretical uncertainties reach approximately the same precision. In Fig. 14(b) we show in magenta the points that will be excluded under the projection considered in Ref. [16]: $\text{BR}(B_s \rightarrow \mu^+\mu^-)_{\text{proj}} = (3.50 \pm 0.17 \pm 0.17) \times 10^{-9}$, with experimental and theoretical uncertainties added in quadrature. As was mentioned in Sec. 3, it should be noted that there will be considerable overlap between the constraint from $\text{BR}(B_s \rightarrow \mu^+\mu^-)$ and searches for a heavy Higgs decaying to tau pairs.

The projected 90% C.L. sensitivity for XENON-1T in the $(m_\chi, \sigma_p^{\text{SI}})$ plane of the CMSSM was shown in Fig. 7(a) as a dashed magenta line. This corresponds to the excluded points in the $(m_0, m_{1/2})$ plane that are presented in orange in Fig. 14(c). XENON-1T and other tonne-scale detectors will probe the ~ 1 TeV higgsino region in its near entirety, with the exception of the points at large m_0 and $m_{1/2}$.

We finally come to CTA’s sensitivity to γ rays from the GC. We applied the binned likelihood function constructed in [110] to the points of the CMSSM, under the assumption of the Einasto profile for the DM distribution in the GC. The points of the $(m_0, m_{1/2})$ plane excluded at the 95% C.L. by the likelihood function with 500 hours of observation are shown in green in Fig. 14(d). CTA is going to provide a strong constraint in the ~ 1 TeV higgsino region, as well as on the majority of the A -resonance region’s points. The sensitivity of CTA reaches the part of the ~ 1 TeV higgsino region that lies outside the sensitivity of tonne-scale underground DM detectors and provides complementary probe to the rest of the parameter space with the exception of the stau-coannihilation region.

To conclude, in Fig. 15 we show the combination of the constraints presented in the panels of Fig. 14. We want to point out that there is no single gray point left in the figure. Since the posterior sample shown contains approximately 20000 points, this implies that even regions well beyond the 95% credible level will be constrained. In addition, Fig. 15 highlights the considerable amount of overlapping between the parameter space probed by CTA and that of other experiments, so that for most of the parameter space detection/exclusion will not rely on a single measurement.

In this regard, we want to point out that if one adopts a flatter profile than the Einasto for the DM distribution in the halo, the above projection for CTA will inevitably be weakened. We have checked that under the NFW profile assumption most points belonging to the A -resonance region and those included in the 68% credible part of the ~ 1 TeV

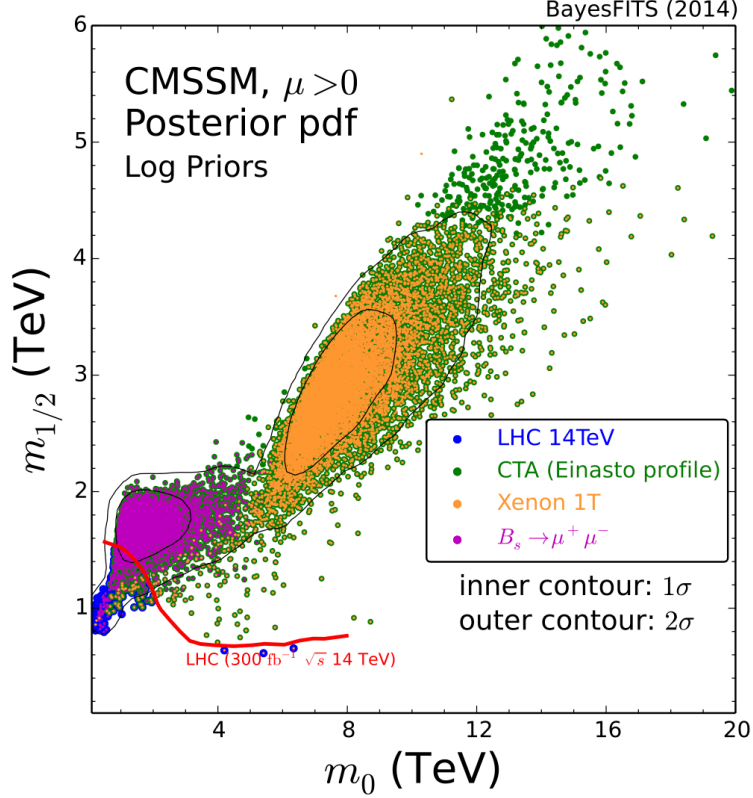


Figure 15: Marginalized 2D posterior in the $(m_0, m_{1/2})$ plane of the CMSSM with $\mu > 0$. 68% and 95% credible regions are shown by the inner and outer contours, respectively. Points are distributed according to the posterior probability. The projected LHC Run II 95% C.L. exclusion line is shown in red solid for reference. Colored points show the future sensitivity to direct SUSY searches in blue, measurement of BR ($B_s \rightarrow \mu^+ \mu^-$) in magenta, tonne-scale underground detectors in orange, and CTA in green.

higgsino region will be excluded. However, most points belonging to the 95% part of the ~ 1 TeV higgsino region, and those characterized by even larger m_0 and $m_{1/2}$ will be beyond reach. Even so, CTA is going to provide an invaluable instrument for complementary testing of the regions of parameter space shown in Figs. 14(b) and 14(c), that will be probed at the LHC and in tonne-scale underground detectors.

References

- [1] **ATLAS** Collaboration, G. Aad et al., *Observation of a new particle in the search for the Standard Model Higgs boson with the ATLAS detector at the LHC*, *Phys.Lett.* **B716** (2012) 1–29, [[arXiv:1207.7214](#)].
- [2] **CMS** Collaboration, S. Chatrchyan et al., *Observation of a new boson at a mass of 125 GeV with the CMS experiment at the LHC*, *Phys.Lett.* **B716** (2012) 30–61, [[arXiv:1207.7235](#)].
- [3] G. L. Kane, C. F. Kolda, L. Roszkowski, and J. D. Wells, *Study of constrained minimal supersymmetry*, *Phys.Rev.* **D49** (1994) 6173–6210, [[hep-ph/9312272](#)].

- [4] H. Baer, V. Barger, and A. Mustafayev, *Implications of a 125 GeV Higgs scalar for LHC SUSY and neutralino dark matter searches*, *Phys.Rev.* **D85** (2012) 075010, [[arXiv:1112.3017](#)].
- [5] M. Kadastik, K. Kannike, A. Racioppi, and M. Raidal, *Implications of the 125 GeV Higgs boson for scalar dark matter and for the CMSSM phenomenology*, *JHEP* **1205** (2012) 061, [[arXiv:1112.3647](#)].
- [6] J. Cao, Z. Heng, D. Li, and J. M. Yang, *Current experimental constraints on the lightest Higgs boson mass in the constrained MSSM*, *Phys.Lett.* **B710** (2012) 665–670, [[arXiv:1112.4391](#)].
- [7] J. Ellis and K. A. Olive, *Revisiting the Higgs Mass and Dark Matter in the CMSSM*, *Eur.Phys.J.* **C72** (2012) 2005, [[arXiv:1202.3262](#)].
- [8] H. Baer, V. Barger, and A. Mustafayev, *Neutralino dark matter in mSUGRA/CMSSM with a 125 GeV light Higgs scalar*, *JHEP* **1205** (2012) 091, [[arXiv:1202.4038](#)].
- [9] P. Bechtle, T. Bringmann, K. Desch, H. Dreiner, M. Hamer, et al., *Constrained Supersymmetry after two years of LHC data: a global view with Fittino*, *JHEP* **1206** (2012) 098, [[arXiv:1204.4199](#)].
- [10] C. Balazs, A. Buckley, D. Carter, B. Farmer, and M. White, *Should we still believe in constrained supersymmetry?*, *Eur.Phys.J.* **C73** (2013) 2563, [[arXiv:1205.1568](#)].
- [11] A. Fowlie, M. Kazana, K. Kowalska, S. Munir, L. Roszkowski, et al., *The CMSSM Favoring New Territories: The Impact of New LHC Limits and a 125 GeV Higgs*, *Phys.Rev.* **D86** (2012) 075010, [[arXiv:1206.0264](#)].
- [12] S. Akula, P. Nath, and G. Peim, *Implications of the Higgs Boson Discovery for mSUGRA*, *Phys.Lett.* **B717** (2012) 188–192, [[arXiv:1207.1839](#)].
- [13] O. Buchmueller, R. Cavanaugh, M. Citron, A. De Roeck, M. Dolan, et al., *The CMSSM and NUHM1 in Light of 7 TeV LHC, B_s to $\mu\mu$ - and XENON100 Data*, *Eur.Phys.J.* **C72** (2012) 2243, [[arXiv:1207.7315](#)].
- [14] C. Stenge, G. Bertone, F. Feroz, M. Fornasa, R. Ruiz de Austri, et al., *Global Fits of the cMSSM and NUHM including the LHC Higgs discovery and new XENON100 constraints*, *JCAP* **1304** (2013) 013, [[arXiv:1212.2636](#)].
- [15] M. E. Cabrera, J. A. Casas, and R. R. de Austri, *The health of SUSY after the Higgs discovery and the XENON100 data*, *JHEP* **1307** (2013) 182, [[arXiv:1212.4821](#)].
- [16] K. Kowalska, L. Roszkowski, and E. M. Sessolo, *Two ultimate tests of constrained supersymmetry*, *JHEP* **1306** (2013) 078, [[arXiv:1302.5956](#)].
- [17] A. Dighe, D. Ghosh, K. M. Patel, and S. Raychaudhuri, *Testing Times for Supersymmetry: Looking Under the Lamp Post*, *Int.J.Mod.Phys.* **A28** (2013) 1350134, [[arXiv:1303.0721](#)].
- [18] T. Cohen and J. G. Wacker, *Here be Dragons: The Unexplored Continents of the CMSSM*, *JHEP* **1309** (2013) 061, [[arXiv:1305.2914](#)].
- [19] **Planck** Collaboration, P. Ade et al., *Planck 2013 results. XVI. Cosmological parameters*, *Astron.Astrophys.* **571** (2014) A16, [[arXiv:1303.5076](#)].
- [20] <http://www.slac.stanford.edu/xorg/hfag/rare/2012/rad11/index.html>.
- [21] **Belle** Collaboration, I. Adachi et al., *Evidence for $B^- \rightarrow \tau^- \bar{\nu}_\tau$ with a Hadronic Tagging*

- Method Using the Full Data Sample of Belle*, *Phys.Rev.Lett.* **110** (2013), no. 13 131801, [[arXiv:1208.4678](#)].
- [22] **LHCb** Collaboration, R. Aaij et al., *Measurement of the $B_s^0 \rightarrow \mu^+ \mu^-$ branching fraction and search for $B^0 \rightarrow \mu^+ \mu^-$ decays at the LHCb experiment*, *Phys.Rev.Lett.* **111** (2013) 101805, [[arXiv:1307.5024](#)].
 - [23] **CMS** Collaboration, S. Chatrchyan et al., *Measurement of the $B(s)$ to $\mu^+ \mu^-$ branching fraction and search for B^0 to $\mu^+ \mu^-$ with the CMS Experiment*, *Phys.Rev.Lett.* **111** (2013) 101804, [[arXiv:1307.5025](#)].
 - [24] **Muon G-2** Collaboration, G. Bennett et al., *Final Report of the Muon E821 Anomalous Magnetic Moment Measurement at BNL*, *Phys.Rev.* **D73** (2006) 072003, [[hep-ex/0602035](#)].
 - [25] J. P. Miller, E. de Rafael, and B. L. Roberts, *Muon ($g-2$): Experiment and theory*, *Rept.Prog.Phys.* **70** (2007) 795, [[hep-ph/0703049](#)].
 - [26] **CMS** Collaboration, S. Chatrchyan et al., *Inclusive search for supersymmetry using the razor variables in pp collisions at $\sqrt{s} = 7$ TeV*, *Phys.Rev.Lett.* **111** (2013), no. 8 081802, [[arXiv:1212.6961](#)].
 - [27] **CMS** Collaboration, S. Chatrchyan et al., *Search for supersymmetry in hadronic final states with missing transverse energy using the variables $\text{Alpha}T$ and b -quark multiplicity in pp collisions at 8 TeV*, *Eur.Phys.J.* **C73** (2013) 2568, [[arXiv:1303.2985](#)].
 - [28] S. Profumo and C. E. Yaguna, *A Statistical analysis of supersymmetric dark matter in the MSSM after WMAP*, *Phys.Rev.* **D70** (2004) 095004, [[hep-ph/0407036](#)].
 - [29] N. Arkani-Hamed, A. Delgado, and G. Giudice, *The Well-tempered neutralino*, *Nucl.Phys.* **B741** (2006) 108–130, [[hep-ph/0601041](#)].
 - [30] L. Roszkowski, R. Ruiz de Austri, R. Trotta, Y.-L. S. Tsai, and T. A. Varley, *Global fits of the Non-Universal Higgs Model*, *Phys.Rev.* **D83** (2011) 015014, [[arXiv:0903.1279](#)].
 - [31] A. Fowlie, K. Kowalska, L. Roszkowski, E. M. Sessolo, and Y.-L. S. Tsai, *Dark matter and collider signatures of the MSSM*, *Phys.Rev.* **D88** (2013), no. 5 055012, [[arXiv:1306.1567](#)].
 - [32] A. Kaminska, G. G. Ross, and K. Schmidt-Hoberg, *Non-universal gaugino masses and fine tuning implications for SUSY searches in the MSSM and the GNMSSM*, *JHEP* **1311** (2013) 209, [[arXiv:1308.4168](#)].
 - [33] K. Kowalska, L. Roszkowski, E. M. Sessolo, and S. Trojanowski, *Low fine tuning in the MSSM with higgsino dark matter and unification constraints*, *JHEP* **1404** (2014) 166, [[arXiv:1402.1328](#)].
 - [34] B. Acharya, M. Actis, T. Aghajani, G. Agnetta, J. Aguilar, et al., *Introducing the CTA concept*, *Astropart.Phys.* **43** (2013) 3–18.
 - [35] **CTA** Collaboration, M. Doro et al., *Dark Matter and Fundamental Physics with the Cherenkov Telescope Array*, *Astropart.Phys.* **43** (2013) 189–214, [[arXiv:1208.5356](#)].
 - [36] M. Pierre, J. M. Siegal-Gaskins, and P. Scott, *Sensitivity of CTA to dark matter signals from the Galactic Center*, *JCAP* **1406** (2014), no. 10 024, [[arXiv:1401.7330](#)].
 - [37] B. Allanach, *SOFTSUSY: a program for calculating supersymmetric spectra*, *Comput.Phys.Commun.* **143** (2002) 305–331, [[hep-ph/0104145](#)].
 - [38] A. Djouadi, J.-L. Kneur, and G. Moultaka, *SuSpect: A Fortran code for the supersymmetric*

- and Higgs particle spectrum in the MSSM, *Comput.Phys.Commun.* **176** (2007) 426–455, [[hep-ph/0211331](#)].
- [39] W. Porod, *SPheno, a program for calculating supersymmetric spectra, SUSY particle decays and SUSY particle production at e^+e^- colliders*, *Comput.Phys.Commun.* **153** (2003) 275–315, [[hep-ph/0301101](#)].
 - [40] S. Heinemeyer, W. Hollik, and G. Weiglein, *The Masses of the neutral CP - even Higgs bosons in the MSSM: Accurate analysis at the two loop level*, *Eur.Phys.J.* **C9** (1999) 343–366, [[hep-ph/9812472](#)].
 - [41] S. Heinemeyer, W. Hollik, and G. Weiglein, *FeynHiggs: A Program for the calculation of the masses of the neutral CP even Higgs bosons in the MSSM*, *Comput.Phys.Commun.* **124** (2000) 76–89, [[hep-ph/9812320](#)].
 - [42] G. Degrandi, S. Heinemeyer, W. Hollik, P. Slavich, and G. Weiglein, *Towards high precision predictions for the MSSM Higgs sector*, *Eur.Phys.J.* **C28** (2003) 133–143, [[hep-ph/0212020](#)].
 - [43] M. Frank, T. Hahn, S. Heinemeyer, W. Hollik, H. Rzehak, et al., *The Higgs Boson Masses and Mixings of the Complex MSSM in the Feynman-Diagrammatic Approach*, *JHEP* **0702** (2007) 047, [[hep-ph/0611326](#)].
 - [44] S. P. Martin, *Three-loop corrections to the lightest Higgs scalar boson mass in supersymmetry*, *Phys.Rev.* **D75** (2007) 055005, [[hep-ph/0701051](#)].
 - [45] R. Harlander, P. Kant, L. Mihaila, and M. Steinhauser, *Higgs boson mass in supersymmetry to three loops*, *Phys.Rev.Lett.* **100** (2008) 191602, [[arXiv:0803.0672](#)].
 - [46] P. Kant, R. Harlander, L. Mihaila, and M. Steinhauser, *Light MSSM Higgs boson mass to three-loop accuracy*, *JHEP* **1008** (2010) 104, [[arXiv:1005.5709](#)].
 - [47] T. Hahn, S. Heinemeyer, W. Hollik, H. Rzehak, and G. Weiglein, *High-Precision Predictions for the Light CP -Even Higgs Boson Mass of the Minimal Supersymmetric Standard Model*, *Phys.Rev.Lett.* **112** (2014), no. 14 141801, [[arXiv:1312.4937](#)].
 - [48] P. Draper, G. Lee, and C. E. M. Wagner, *Precise estimates of the Higgs mass in heavy supersymmetry*, *Phys.Rev.* **D89** (2014), no. 5 055023, [[arXiv:1312.5743](#)].
 - [49] J. L. Feng, P. Kant, S. Profumo, and D. Sanford, *Three-Loop Corrections to the Higgs Boson Mass and Implications for Supersymmetry at the LHC*, *Phys.Rev.Lett.* **111** (2013) 131802, [[arXiv:1306.2318](#)].
 - [50] O. Buchmueller, M. Dolan, J. Ellis, T. Hahn, S. Heinemeyer, et al., *Implications of Improved Higgs Mass Calculations for Supersymmetric Models*, *Eur.Phys.J.* **C74** (2014) 2809, [[arXiv:1312.5233](#)].
 - [51] O. Buchmueller, R. Cavanaugh, A. De Roeck, M. Dolan, J. Ellis, et al., *The CMSSM and NUHM1 after LHC Run 1*, *Eur.Phys.J.* **C74** (2014), no. 6 2922, [[arXiv:1312.5250](#)].
 - [52] **LUX** Collaboration, D. Akerib et al., *First results from the LUX dark matter experiment at the Sanford Underground Research Facility*, *Phys.Rev.Lett.* **112** (2014), no. 9 091303, [[arXiv:1310.8214](#)].
 - [53] A. Fowlie, A. Kalinowski, M. Kazana, L. Roszkowski, and Y. S. Tsai, *Bayesian Implications of Current LHC and XENON100 Search Limits for the Constrained MSSM*, *Phys.Rev.* **D85** (2012) 075012, [[arXiv:1111.6098](#)].

- [54] L. Roszkowski, E. M. Sessolo, and Y.-L. S. Tsai, *Bayesian Implications of Current LHC Supersymmetry and Dark Matter Detection Searches for the Constrained MSSM*, *Phys.Rev.* **D86** (2012) 095005, [[arXiv:1202.1503](#)].
- [55] P. Bechtle, S. Heinemeyer, O. Stl, T. Stefaniak, and G. Weiglein, *HiggsSignals: Confronting arbitrary Higgs sectors with measurements at the Tevatron and the LHC*, *Eur.Phys.J.* **C74** (2014), no. 2 2711, [[arXiv:1305.1933](#)].
- [56] P. Bechtle, O. Brein, S. Heinemeyer, G. Weiglein, and K. E. Williams, *HiggsBounds: Confronting Arbitrary Higgs Sectors with Exclusion Bounds from LEP and the Tevatron*, *Comput.Phys.Commun.* **181** (2010) 138–167, [[arXiv:0811.4169](#)].
- [57] P. Bechtle, O. Brein, S. Heinemeyer, G. Weiglein, and K. E. Williams, *HiggsBounds 2.0.0: Confronting Neutral and Charged Higgs Sector Predictions with Exclusion Bounds from LEP and the Tevatron*, *Comput.Phys.Commun.* **182** (2011) 2605–2631, [[arXiv:1102.1898](#)].
- [58] P. Bechtle, O. Brein, S. Heinemeyer, O. Stål, T. Stefaniak, et al., *HiggsBounds-4: Improved Tests of Extended Higgs Sectors against Exclusion Bounds from LEP, the Tevatron and the LHC*, *Eur.Phys.J.* **C74** (2014) 2693, [[arXiv:1311.0055](#)].
- [59] M. Drees, H. Dreiner, D. Schmeier, J. Tattersall, and J. S. Kim, *CheckMATE: Confronting your Favourite New Physics Model with LHC Data*, *Comput.Phys.Commun.* **187** (2014) 227–265, [[arXiv:1312.2591](#)].
- [60] A. Barr, C. Lester, and P. Stephens, *$m(T2)$: The Truth behind the glamour*, *J.Phys.* **G29** (2003) 2343–2363, [[hep-ph/0304226](#)].
- [61] H.-C. Cheng and Z. Han, *Minimal Kinematic Constraints and $m(T2)$* , *JHEP* **0812** (2008) 063, [[arXiv:0810.5178](#)].
- [62] M. Cacciari and G. P. Salam, *Dispelling the N^3 myth for the k_t jet-finder*, *Phys.Lett.* **B641** (2006) 57–61, [[hep-ph/0512210](#)].
- [63] M. Cacciari, G. P. Salam, and G. Soyez, *The Anti- $k(t)$ jet clustering algorithm*, *JHEP* **0804** (2008) 063, [[arXiv:0802.1189](#)].
- [64] M. Cacciari, G. P. Salam, and G. Soyez, *FastJet User Manual*, *Eur.Phys.J.* **C72** (2012) 1896, [[arXiv:1111.6097](#)].
- [65] **DELPHES 3** Collaboration, J. de Favereau et al., *DELPHES 3, A modular framework for fast simulation of a generic collider experiment*, *JHEP* **1402** (2014) 057, [[arXiv:1307.6346](#)].
- [66] C. Lester and D. Summers, *Measuring masses of semiinvisibly decaying particles pair produced at hadron colliders*, *Phys.Lett.* **B463** (1999) 99–103, [[hep-ph/9906349](#)].
- [67] A. L. Read, *Presentation of search results: The $CL(s)$ technique*, *J.Phys.* **G28** (2002) 2693–2704.
- [68] **Particle Data Group** Collaboration, J. Beringer et al., *Review of Particle Physics (RPP)*, *Phys.Rev.* **D86** (2012) 010001.
- [69] K. Cheung, Y.-L. S. Tsai, P.-Y. Tseng, T.-C. Yuan, and A. Zee, *Global Study of the Simplest Scalar Phantom Dark Matter Model*, *JCAP* **1210** (2012) 042, [[arXiv:1207.4930](#)].
- [70] **XENON100** Collaboration, E. Aprile et al., *Dark Matter Results from 225 Live Days of XENON100 Data*, *Phys.Rev.Lett.* **109** (2012) 181301, [[arXiv:1207.5988](#)].

- [71] G. Belanger, F. Boudjema, A. Pukhov, and A. Semenov, *micrOMEGAs 3: A program for calculating dark matter observables*, *Comput.Phys.Commun.* **185** (2014) 960–985, [[arXiv:1305.0237](#)].
- [72] J. R. Ellis, K. A. Olive, and C. Savage, *Hadronic Uncertainties in the Elastic Scattering of Supersymmetric Dark Matter*, *Phys.Rev.* **D77** (2008) 065026, [[arXiv:0801.3656](#)].
- [73] R. Young, *Strange quark content of the nucleon and dark matter searches*, *PoS LATTICE2012* (2012) 014, [[arXiv:1301.1765](#)].
- [74] J. Alwall, M. Herquet, F. Maltoni, O. Mattelaer, and T. Stelzer, *MadGraph 5 : Going Beyond*, *JHEP* **1106** (2011) 128, [[arXiv:1106.0522](#)].
- [75] T. Sjostrand, S. Mrenna, and P. Z. Skands, *A Brief Introduction to PYTHIA 8.1*, *Comput.Phys.Commun.* **178** (2008) 852–867, [[arXiv:0710.3820](#)].
- [76] W. Beenakker, R. Hopker, M. Spira, and P. Zerwas, *Squark and gluino production at hadron colliders*, *Nucl.Phys.* **B492** (1997) 51–103, [[hep-ph/9610490](#)].
- [77] A. Kulesza and L. Motyka, *Threshold resummation for squark-antisquark and gluino-pair production at the LHC*, *Phys.Rev.Lett.* **102** (2009) 111802, [[arXiv:0807.2405](#)].
- [78] A. Kulesza and L. Motyka, *Soft gluon resummation for the production of gluino-gluino and squark-antisquark pairs at the LHC*, *Phys.Rev.* **D80** (2009) 095004, [[arXiv:0905.4749](#)].
- [79] W. Beenakker, S. Brensing, M. Kramer, A. Kulesza, E. Laenen, et al., *Soft-gluon resummation for squark and gluino hadroproduction*, *JHEP* **0912** (2009) 041, [[arXiv:0909.4418](#)].
- [80] W. Beenakker, S. Brensing, M. Kramer, A. Kulesza, E. Laenen, et al., *Squark and Gluino Hadroproduction*, *Int.J.Mod.Phys.* **A26** (2011) 2637–2664, [[arXiv:1105.1110](#)].
- [81] **ATLAS** Collaboration, *Search for squarks and gluinos with the ATLAS detector in final states with jets and missing transverse momentum and 20.3 fb⁻¹ of $\sqrt{s} = 8$ TeV proton-proton collision data*, Tech. Rep. ATLAS-CONF-2013-047, CERN, Geneva, May, 2013.
- [82] **ATLAS** Collaboration, *Search for strong production of supersymmetric particles in final states with missing transverse momentum and at least three b-jets using 20.1 fb1 of pp collisions at $\sqrt{s} = 8$ TeV with the ATLAS Detector.*, Tech. Rep. ATLAS-CONF-2013-061, CERN, Geneva, Jun, 2013.
- [83] K. N. Abazajian and J. P. Harding, *Constraints on WIMP and Sommerfeld-Enhanced Dark Matter Annihilation from HESS Observations of the Galactic Center*, *JCAP* **1201** (2012) 041, [[arXiv:1110.6151](#)].
- [84] **Fermi-LAT** Collaboration, M. Ackermann et al., *Dark Matter Constraints from Observations of 25 Milky Way Satellite Galaxies with the Fermi Large Area Telescope*, *Phys.Rev.* **D89** (2014) 042001, [[arXiv:1310.0828](#)].
- [85] K. Bernl  hr, A. Barnacka, Y. Becherini, O. Blanch Bigas, E. Carmona, et al., *Monte Carlo design studies for the Cherenkov Telescope Array*, *Astropart.Phys.* **43** (2013) 171–188, [[arXiv:1210.3503](#)].
- [86] K. Kowalska et al., *Constrained next-to-minimal supersymmetric standard model with a 126 GeV Higgs boson: A global analysis*, *Phys.Rev.* **D87** (2013), no. 11 115010, [[arXiv:1211.1693](#)].

- [87] F. Feroz, M. Hobson, and M. Bridges, *MultiNest: an efficient and robust Bayesian inference tool for cosmology and particle physics*, *Mon.Not.Roy.Astron.Soc.* **398** (2009) 1601–1614, [[arXiv:0809.3437](#)].
- [88] F. Mahmoudi, *SuperIso v2.3: A Program for calculating flavor physics observables in Supersymmetry*, *Comput.Phys.Commun.* **180** (2009) 1579–1613, [[arXiv:0808.3144](#)].
- [89] C. Bobeth, M. Gorbahn, T. Hermann, M. Misiak, E. Stamou, et al., *$B_{s,d} \rightarrow l^+ l^-$ in the Standard Model with Reduced Theoretical Uncertainty*, *Phys.Rev.Lett.* **112** (2014) 101801, [[arXiv:1311.0903](#)].
- [90] **ATLAS, CDF, CMS, D0** Collaboration, *First combination of Tevatron and LHC measurements of the top-quark mass*, [arXiv:1403.4427](#).
- [91] J. R. Ellis, T. Falk, and K. A. Olive, *Neutralino - Stau coannihilation and the cosmological upper limit on the mass of the lightest supersymmetric particle*, *Phys.Lett.* **B444** (1998) 367–372, [[hep-ph/9810360](#)].
- [92] M. Drees and M. M. Nojiri, *The Neutralino relic density in minimal $N = 1$ supergravity*, *Phys.Rev.* **D47** (1993) 376–408, [[hep-ph/9207234](#)].
- [93] K. L. Chan, U. Chattopadhyay, and P. Nath, *Naturalness, weak scale supersymmetry and the prospect for the observation of supersymmetry at the Tevatron and at the CERN LHC*, *Phys.Rev.* **D58** (1998) 096004, [[hep-ph/9710473](#)].
- [94] J. L. Feng, K. T. Matchev, and T. Moroi, *Multi - TeV scalars are natural in minimal supergravity*, *Phys.Rev.Lett.* **84** (2000) 2322–2325, [[hep-ph/9908309](#)].
- [95] J. L. Feng, K. T. Matchev, and T. Moroi, *Focus points and naturalness in supersymmetry*, *Phys.Rev.* **D61** (2000) 075005, [[hep-ph/9909334](#)].
- [96] **WMAP** Collaboration, E. Komatsu et al., *Seven-Year Wilkinson Microwave Anisotropy Probe (WMAP) Observations: Cosmological Interpretation*, *Astrophys.J.Suppl.* **192** (2011) 18, [[arXiv:1001.4538](#)].
- [97] **ATLAS** Collaboration, *Prospects for benchmark Supersymmetry searches at the high luminosity LHC with the ATLAS Detector*, Tech. Rep. ATL-PHYS-PUB-2013-011, CERN, Geneva, Sep, 2013.
- [98] T. Cohen, T. Golling, M. Hance, A. Henrichs, K. Howe, et al., *SUSY Simplified Models at 14, 33, and 100 TeV Proton Colliders*, *JHEP* **1404** (2014) 117, [[arXiv:1311.6480](#)].
- [99] A. Arbey, M. Battaglia, and F. Mahmoudi, *Supersymmetric Heavy Higgs Bosons at the LHC*, *Phys.Rev.* **D88** (2013), no. 1 015007, [[arXiv:1303.7450](#)].
- [100] **CMS** Collaboration, *Higgs to tau tau (MSSM) (HCP)*, Tech. Rep. CMS-PAS-HIG-12-050, CERN, Geneva, 2012.
- [101] M. S. Carena, S. Heinemeyer, C. Wagner, and G. Weiglein, *Suggestions for benchmark scenarios for MSSM Higgs boson searches at hadron colliders*, *Eur.Phys.J.* **C26** (2003) 601–607, [[hep-ph/0202167](#)].
- [102] A. Djouadi and J. Quevillon, *The MSSM Higgs sector at a high M_{SUSY} : reopening the low $\tan\beta$ regime and heavy Higgs searches*, *JHEP* **1310** (2013) 028, [[arXiv:1304.1787](#)].
- [103] **XENON1T** Collaboration, E. Aprile, *The XENON1T Dark Matter Search Experiment*, *Springer Proc.Phys.* **C12-02-22** (2013) 93–96, [[arXiv:1206.6288](#)].

- [104] M. Wood, J. Buckley, S. Digel, S. Funk, D. Nieto, et al., *Prospects for Indirect Detection of Dark Matter with CTA*, [arXiv:1305.0302](#).
- [105] J. F. Navarro, C. S. Frenk, and S. D. White, *The Structure of cold dark matter halos*, *Astrophys.J.* **462** (1996) 563–575, [[astro-ph/9508025](#)].
- [106] J. Einasto, *On the Construction of a Composite Model for the Galaxy and on the Determination of the System of Galactic Parameters*, *Trudy Astrofizicheskogo Instituta Alma-Ata* **5** (1965) 87–100.
- [107] B. Cabrera, L. M. Krauss, and F. Wilczek, *Bolometric Detection of Neutrinos*, *Phys.Rev.Lett.* **55** (1985) 25.
- [108] J. Monroe and P. Fisher, *Neutrino Backgrounds to Dark Matter Searches*, *Phys.Rev.* **D76** (2007) 033007, [[arXiv:0706.3019](#)].
- [109] J. Billard, L. Strigari, and E. Figueroa-Feliciano, *Implication of neutrino backgrounds on the reach of next generation dark matter direct detection experiments*, *Phys.Rev.* **D89** (2014) 023524, [[arXiv:1307.5458](#)].
- [110] L. Roszkowski, E. M. Sessolo, and A. J. Williams, *Prospects for dark matter searches in the $pMSSM$* , [arXiv:1411.5214](#).
- [111] H. Baer, V. Barger, A. Lessa, and X. Tata, *SUSY discovery potential of LHC14 with $0.3 - 3 \sim ab^{-1}$: A Snowmass whitepaper*, [arXiv:1306.5343](#).